

SINGLE INDEX FRÉCHET REGRESSION

Satarupa Bhattacharjee and Hans-Georg Müller¹
 Department of Statistics, University of California, Davis
 Davis, CA 95616

August, 2021

ABSTRACT

Single index models provide an effective dimension reduction tool in regression, especially for high dimensional data, by projecting a general multivariate predictor onto a direction vector. We propose a novel single-index model for regression models where metric space-valued random object responses are coupled with multivariate Euclidean predictors. The responses in this regression model include complex, non-Euclidean data, including covariance matrices, graph Laplacians of networks and univariate probability distribution functions among other complex objects that lie in abstract metric spaces. Fréchet regression has provided an approach for modeling the conditional mean of such random objects given multivariate Euclidean vectors, but it does not provide for regression parameters such as slopes or intercepts, since the metric space-valued responses are not amenable to linear operations. We show here that for the case of multivariate Euclidean predictors, the parameters that define a single index and associated projection vector can be used to substitute for the inherent absence of parameters in Fréchet regression. Specifically, we derive the asymptotic consistency of suitable estimates of these parameters subject to an identifiability condition. Consistent estimation of the link function of the single index Fréchet regression model is obtained through local Fréchet regression. We demonstrate the finite sample performance of estimation for the proposed single index Fréchet regression model through simulation studies, including the special cases of probability distributions and graph adjacency matrices. The method is also illustrated for resting state functional Magnetic Resonance Imaging (fMRI) data from the ADNI study.

KEY WORDS: Single index, Dimension reduction, non-Euclidean object data, local Fréchet regression, M-estimation, fMRI.

¹Research supported in part by NSF grant DMS-2014626 and an NIH ECHO grant.

1 Introduction

Modeling the regression relationship between a response Y and a multivariate Euclidean predictor vector \mathbf{X} corresponds to specifying the form of the conditional means $h(\mathbf{x}) = \mathbb{E}(Y|\mathbf{X} = \mathbf{x})$ and higher dimensionality of \mathbf{X} can be problematic when one is interested to go beyond the standard multiple linear model. This provides strong motivation to consider regression models that provide dimension reduction, and single index models are one of the most popular approaches to achieve this, under the assumption that the influence of the predictors can be collapsed to an index, i.e., a projection on one direction complemented by a nonparametric link function. This reduces the predictors to a univariate index while still capturing relevant features of the high-dimensional data and is thus not subject to the curse of dimensionality. This model generalizes linear regression (where the link function is the identity) and is a special case of nonparametric regression (Heckman, 1986; Rice, 1986; Ruppert et al., 2003), which in its general form is subject to the curse of dimensionality. For a real-valued response Y and a p -dimensional predictor \mathbf{X} , the semiparametric single index regression model is

$$\mathbb{E}(Y|\mathbf{X} = \mathbf{x}) = m(\mathbf{x}^\top \bar{\boldsymbol{\theta}}_0). \quad (1)$$

In model (1), the dependence between Y and \mathbf{X} is characterized by the conditional mean, i.e., the conditional mean is a function of $\bar{\boldsymbol{\theta}}_0$, and this reduces the dimensionality of the predictor from p to essentially 1.

The function $m(\cdot)$ is nonparametric and thus includes location and level changes, and therefore the vector \mathbf{X}_i cannot include a constant that would serve as intercept. For identifiability reasons, $\bar{\boldsymbol{\theta}}_0$ is often assumed to be a unit vector with non-negative first coordinate. A second approach that has been used is to require one component to equal one. This presupposes that the component that is set to equal 1 indeed has a non-zero coefficient (Lin and Kulasekera, 2007; Cui et al., 2011; Ichimura, 1993). Model (1) is only meaningful if the Euclidean predictor vector \mathbf{X}_i is of dimension 2 or larger. If \mathbf{X}_i is one-dimensional, the corresponding special case of the model is the one-dimensional nonparametric regression $\mathbb{E}(Y|X = x) = m(x)$, which does not feature any parametric component.

Due to its flexibility, the interpretability of the (linear) coefficients and the nonparametric link function $m(\cdot)$, as well as due to its wide applicability in many scientific fields, the classical single index regression model with Euclidean responses has attracted attention from the scientific community for a long time. The coefficient $\bar{\boldsymbol{\theta}}_0$ that defines the single index $\mathbf{x}^\top \bar{\boldsymbol{\theta}}_0$ along with the shape of the nonparametric component $m(\cdot)$ characterizes the relationship between the response and the predictor. The parametric component $\bar{\boldsymbol{\theta}}_0$ is of primary interest in this model. The problem of recovering the true direction $\bar{\boldsymbol{\theta}}_0$ can be viewed as a subclass

of sufficient dimension reduction (SDR) techniques, where identifying the central subspace of \mathbf{X} that explains most of the variation in Y has been a prime target (Chen and Li, 1998; Li and Duan, 1989; Cook, 1994; Li and Wang, 2007).

In addition to sufficient dimension reduction techniques, a multitude of related approaches to estimate $\bar{\theta}_0$ in (1) have been studied. These include projection pursuit regression (PPR) (Friedman and Stuetzle, 1981; Hall, 1989), the average derivative approach (Härdle and Stoker, 1989; Stoker, 1986; Fan, 1995; Powell et al., 1986), sliced inverse regression (SIR) (Li, 1991; Cook and Weisberg, 1991), conditional minimum average variance estimation (MAVE) (Xia et al., 2009) and various other methods (Wang et al., 2010; Xia and Li, 1999; Xia, 2006, 2007; Liang et al., 2010; Yu and Ruppert, 2002). Various approaches focused on nonparametric estimation of the link function to recover the index parameter in (1) (Härdle et al., 1993; Huh and Park, 2002; Hristache et al., 2001) along with partially linear versions (Carroll et al., 1997; Cui et al., 2011; Ichimura, 1993), various noise models (Chang et al., 2010; Wang et al., 2010).

Various extensions of single index regression have been considered more recently (Zhao et al., 2020; Kereta et al., 2020), including models with multiple indices or high-dimensional predictors (Zhu and Zhu, 2009; Zhou and He, 2008; Kuchibhotla et al., 2017; Kuchibhotla and Patra, 2020) and longitudinal and functional data as predictors (Jiang and Wang, 2011; Chen et al., 2011; Ferraty et al., 2011; Novo et al., 2019). However, none of these extensions considers the case where responses are not in a Euclidean vector space, even though this case is increasingly important for data application. An exception is Ying and Yu (2020), who considered extending sufficient dimension reduction approaches for the case of random objects. This lack of available methodology for single index models with random object responses motivates our approach. Non-Euclidean complex data structures arising in areas such as biological or social sciences are becoming increasingly common, due to technological advances have made it possible to record and efficiently store time courses of images (Peyré, 2009; González-Briones et al., 2018), shapes (Small, 2012) or networks (Tsochantaridis et al., 2004), in addition to sensor data and other complex data. For example, one might be interested in the functional connectivity quantified as correlation matrices obtained from neuroimaging studies to study the effect of predictors on brain connectivity, an application that we explore further below.

Other examples of general metric space objects include probability distributions (Delicado and Vieu, 2017), such as age-at-death distributions as observed in demography or network objects, such as internet traffic networks. Such “object-oriented data” (Marron and Alonso, 2014) or “random objects” (Müller, 2016) can be viewed as random variables taking values in a separable metric space that is devoid of a vector space structure and where only

pairwise distances between the observed data are available. Existing methodology for single index models as briefly reviewed above assumes that one has Euclidean responses, and these methods rely in a fundamental way on the vector space structure of the responses. When there is no linear structure, new methodology is needed and this paper contributes to this development.

The natural notion of a mean for random elements of a metric space is the Fréchet mean (Fréchet, 1948), which is a direct generalization of the standard mean, and is defined as the element of the metric space for which the expected squared distance to all other elements, the so-called Fréchet function, is minimized. Depending on the space and metric, Fréchet means may or may not exist as unique minimizers of the Fréchet function. Fréchet regression is an extension of Fréchet means to the notion of conditional Fréchet means, and has been recently studied in several papers (Petersen and Müller, 2019; Dubey and Müller, 2019; Petersen et al., 2019; Chen and Müller, 2018), including both global and local versions.

In this paper, we introduce a novel method for the single Index Fréchet Regression (IFR) when the response variable is a random object lying in a general metric space and the predictor is a p -dimensional Euclidean vector. Our goal is to develop a simple and straightforward extension of the conventional estimation paradigm for single index models for this challenging case. Since there is no notion of direction or sign in a general metric space, we interpret the index parameter in the proposed index Fréchet regression model (IFR) as the direction in the predictor space along which the variability of the response is maximized. It turns out to be useful to view the direction as an M-estimator of an appropriate objective function, and to use empirical process theory to show consistency of the proposed estimate. We also develop a bootstrap method to obtain inference in finite sample situations.

The paper is organized as follows: The basic set up is defined in Section 2 and theory on the asymptotic behavior of the index parameter is provided in Section 3. The index vector is assumed to lie on a hypersphere, with non-negative first element to facilitate identifiability. Then it is natural to quantify the performance of the proposed estimators by the geodesic distances between the estimated and true directions. Empirical studies with different types of random object responses are conducted in Section 4 to validate the estimation method. In Section 5 we apply the methods to infer and analyze the effect of age, sex, total ADAS score, and the stage of propagation of Alzheimer’s Disease (AD) on the brain connectivity networks of patients with dementia. The networks are derived from fMRI signals of certain brain regions (Thomas Yeo et al., 2011) and for our analysis we represent them as correlation matrices. We conclude with a brief discussion in Section 6.

2 Model and estimation methods

More formally, in all of the following (Ω, d, P) is a totally bounded metric space with metric d and probability measure P . The random objects Y take values in Ω . This is coupled with a p -dimensional real-valued predictor \mathbf{X} . The conditional Fréchet mean of $Y|\mathbf{X}$ is a generalization of $\mathbb{E}(Y|\mathbf{X} = \mathbf{x})$ to metric spaces, as the minimizer of $\mathbb{E}(d^2(Y, \omega)|\mathbf{X} = \mathbf{x})$, $\omega \in \Omega$. The latter is the corresponding generalized measure of dispersion around the conditional Fréchet mean and can be viewed as a conditional Fréchet function.

Adopting the framework of Fréchet regression for random objects with Euclidean predictors, we define the Index Fréchet Regression (IFR) model as

$$m_{\oplus}(\mathbf{x}^{\top} \bar{\boldsymbol{\theta}}_0) := \mathbb{E}_{\oplus}(Y|\mathbf{X} = \mathbf{x}) := \underset{\omega \in \Omega}{\operatorname{argmin}} \mathbb{E}(d^2(Y, \omega)|\mathbf{X} = \mathbf{x}), \quad (2)$$

where $\bar{\boldsymbol{\theta}}_0$ is the true direction parameter of interest. The conditional Fréchet mean is assumed to be a function of $\bar{\boldsymbol{\theta}}_0$ in such a way that the distribution of Y only depends on \mathbf{X} through the index $\mathbf{X}^{\top} \bar{\boldsymbol{\theta}}_0$, that is,

$$Y \perp \mathbb{E}(Y|\mathbf{X}) | (\mathbf{X}^{\top} \bar{\boldsymbol{\theta}}_0).$$

Model (1) emerges as a special case of model (2) for a Euclidean response, as the conditional Fréchet mean coincides with the conditional expectation $\mathbb{E}(Y|\mathbf{X})$ for the choice of the squared distance metric for the case $\Omega = \mathbb{R}$.

The identifiability condition for is rephrased following the state-of-the-art literature (Carroll et al., 1997; Lin and Kulasekera, 2007; Cui et al., 2011; Zhu and Xue, 2006). We assume the parameter space to be Θ rather than the entire \mathbb{R}^p in order to ensure that $\boldsymbol{\theta}$ in the representation (3) can be uniquely defined, where $\Theta := \{\bar{\boldsymbol{\theta}} = (\theta_1, \dots, \theta_p)^{\top} : \|\bar{\boldsymbol{\theta}}\| = 1, \theta_1 \geq 0, \bar{\boldsymbol{\theta}} \in \mathbb{R}^p\}$. We first choose an identifiable parametrization which transforms the boundary of a unit ball in \mathbb{R}^p to the interior of a unit ball in $\mathbb{R}^{(p-1)}$. By eliminating θ_1 , the parameter space Θ can be rearranged to a form $\{(1 - \sum_{r=2}^p \theta_r^2)^{1/2}, \theta_2, \dots, \theta_p\}^{\top} : \sum_{r=2}^p \theta_r^2 \leq 1\}$. This re-parametrization is the key to analyzing the asymptotic properties of the estimates for $\boldsymbol{\theta}$ and to facilitating an efficient computation algorithm.

The true parameter is then partitioned into $\bar{\boldsymbol{\theta}} = (\theta_1, \boldsymbol{\theta})^{\top}$, where $\boldsymbol{\theta} = (\theta_2, \dots, \theta_p)^{\top}$. We need to estimate the $(p-1)$ -dimensional vector $\boldsymbol{\theta}$ in the single-index model, and then use the fact that $\theta_1 = (1 - \sum_{r=2}^p \theta_r^2)^{1/2}$ to obtain $\hat{\theta}_1$.

Proposition 1 (Identifiability of model (2)). *Suppose $h_{\oplus}(\mathbf{x}) = \mathbb{E}(Y|\mathbf{X} = \mathbf{x})$. The support S of $h_{\oplus}(\cdot)$ is a convex bounded set with at least one interior point and $h_{\oplus}(\cdot)$ is a non-constant*

continuous function on S . If

$$h_{\oplus}(\mathbf{x}) = g_{1\oplus}(\boldsymbol{\alpha}^\top \mathbf{x}) = g_{2\oplus}(\boldsymbol{\beta}^\top \mathbf{x}), \text{ for all } \mathbf{x} \in S,$$

for some continuous link function objects $g_{1\oplus}$ and $g_{2\oplus}$, and some $\boldsymbol{\alpha}, \boldsymbol{\beta}$ with positive first element such that $\|\boldsymbol{\alpha}\| = \|\boldsymbol{\beta}\| = 1$ then $\boldsymbol{\alpha} = \boldsymbol{\beta}$ and $g_{1\oplus} \equiv g_{2\oplus}$ on $\{\boldsymbol{\alpha}^\top \mathbf{x} | \mathbf{x} \in S\}$.

The above result can be proven using a similar argument as given in Theorem 1 of [Lin and Kulasekera \(2007\)](#).

Studying the special case of the Euclidean response Y in detail one may observe that the variation in Y results from the variation in $\mathbf{X}^\top \bar{\boldsymbol{\theta}}_0$ and also from the variation in the error, ε ([Ichimura, 1993](#)). On the contour line $\mathbf{X}^\top \bar{\boldsymbol{\theta}}_0 = c$, the variability in Y only results from the variability in ε . Along the contour line $\mathbf{X}^\top \bar{\boldsymbol{\theta}}_0 = c$, $\bar{\boldsymbol{\theta}} \neq \bar{\boldsymbol{\theta}}_0$, the value of $\mathbf{X}^\top \bar{\boldsymbol{\theta}}_0$ changes. Therefore the variability in Y on the contour line $\mathbf{X}^\top \bar{\boldsymbol{\theta}}_0 = c$, $\bar{\boldsymbol{\theta}} \neq \bar{\boldsymbol{\theta}}_0$ comes from both the variation in $\mathbf{X}^\top \bar{\boldsymbol{\theta}}_0$ and in ε . Since $\text{Var}(Y | \mathbf{X}^\top \bar{\boldsymbol{\theta}}_0 = c)$ measures the variability in Y on a contour line $\mathbf{X}^\top \bar{\boldsymbol{\theta}}_0 = c$, $\bar{\boldsymbol{\theta}} \neq \bar{\boldsymbol{\theta}}_0$, a sensible way to alternatively interpret $\bar{\boldsymbol{\theta}}_0$ would be finding the minimizer of the objective function $H(\bar{\boldsymbol{\theta}})$, where $H(\bar{\boldsymbol{\theta}}) := \mathbb{E}(\text{Var}(Y | \mathbf{X}^\top \bar{\boldsymbol{\theta}}_0))$ and $\bar{\boldsymbol{\theta}}_0 = \underset{\bar{\boldsymbol{\theta}}: \bar{\boldsymbol{\theta}}^\top \bar{\boldsymbol{\theta}}=1}{\text{argmin}} H(\bar{\boldsymbol{\theta}})$. It is indeed important to impose the constraint $\bar{\boldsymbol{\theta}}^\top \bar{\boldsymbol{\theta}} = 1$, with the first element of the index $\theta_{01} > 0$ to ensure the identifiability of the objective function. Under such constraint we note that $H(\bar{\boldsymbol{\theta}}_0) \leq H(\bar{\boldsymbol{\theta}})$.

The method for recovering the true direction of the single index from model (2) can be generalized in a similar way. The conditional variance of Y given $\mathbf{X} = \mathbf{x}$ for a real-valued response can be directly generalized to the conditional Fréchet variance $d^2(Y, m_{\oplus}(\mathbf{x}^\top \bar{\boldsymbol{\theta}}))$ for any given unit orientation vector $\bar{\boldsymbol{\theta}}$. Thus, for a general object response $Y \in (\Omega, d)$, $\bar{\boldsymbol{\theta}}_0$ can alternatively be expressed as

$$\begin{aligned} \bar{\boldsymbol{\theta}}_0 &= \underset{\bar{\boldsymbol{\theta}} \in \Theta}{\text{argmin}} H(\bar{\boldsymbol{\theta}}), \text{ where } H(\bar{\boldsymbol{\theta}}) = \mathbb{E}(d^2(Y, m_{\oplus}(\mathbf{X}^\top \bar{\boldsymbol{\theta}}))), \\ m_{\oplus}(t) &= \underset{\omega \in \Omega}{\text{argmin}} M(\omega, t), \text{ with } M(\omega, t) := \mathbb{E}(d^2(Y, \omega) | \mathbf{X}^\top \bar{\boldsymbol{\theta}}_0 = t). \end{aligned} \quad (3)$$

To recover $\bar{\boldsymbol{\theta}}_0$ from the representation (3), one needs to also estimate the conditional Fréchet mean, as in the IFR model (2). We employ the local Fréchet regression estimate ([Petersen and Müller, 2019](#)) for this. The conditional Fréchet mean in (3) can be approximated by a locally weighted Fréchet mean, with weight function $S(\cdot, \cdot, \cdot)$ that depends on a chosen kernel function $K(\cdot)$ and a bandwidth parameter b . For any given unit direction index $\bar{\boldsymbol{\theta}}$, this intermediate localized weighted Fréchet mean is defined as

$$\tilde{m}_{\oplus}(t) = \underset{\omega \in \Omega}{\text{argmin}} \tilde{L}_b(\omega, t), \text{ with } \tilde{L}_b(\omega, t) := \mathbb{E}(S(\mathbf{X}^\top \bar{\boldsymbol{\theta}}, t, b) d^2(Y, \omega)), \quad (4)$$

where

$$\begin{aligned} S(\mathbf{X}^\top \bar{\boldsymbol{\theta}}, t, b) &= \frac{1}{\sigma_0^2} K_b(\mathbf{X}^\top \bar{\boldsymbol{\theta}} - t) [\mu_2 - \mu_1(\mathbf{X}^\top \bar{\boldsymbol{\theta}} - t)], \\ \mu_k &= \mathbb{E}(K_b(\mathbf{X}^\top \bar{\boldsymbol{\theta}} - t) (\mathbf{X}^\top \bar{\boldsymbol{\theta}} - t)^k), \quad k = 0, 1, 2, \quad \sigma_0^2 = \mu_2 \mu_0 - \mu_1^2, \end{aligned} \quad (5)$$

where $M(\cdot, t) = \tilde{L}_b(\cdot, t) + O(b)$ for all t (Petersen and Müller, 2019). Suppose we observe a random sample of paired observations (\mathbf{X}_i, Y_i) , $l = 1, \dots, n$, where \mathbf{X}_i is a p -dimensional Euclidean predictor and $Y_i \in (\Omega, d)$ is an object response situated in a general metric space (Ω, d) . Using the form of the intermediate target in (4) and replacing the auxiliary parameters by their corresponding empirical estimates, the local Fréchet regression estimator at a given value t of the single index is defined as

$$\hat{m}_\oplus(t) = \operatorname{argmin}_{\omega \in \Omega} \hat{L}_n(\omega, t), \quad \text{with } \hat{L}_n(\omega, t) := \frac{1}{n} \sum_{i=1}^n \hat{S}(\mathbf{X}_i^\top \bar{\boldsymbol{\theta}}, t, b) d^2(Y_i, \omega), \quad (6)$$

where

$$\begin{aligned} \hat{S}(\mathbf{X}_i^\top \bar{\boldsymbol{\theta}}, t, b) &= \frac{1}{\hat{\sigma}_0^2} K_b(\mathbf{X}_i^\top \bar{\boldsymbol{\theta}} - t) [\hat{\mu}_2 - \hat{\mu}_1(\mathbf{X}_i^\top \bar{\boldsymbol{\theta}} - t)], \\ \hat{\mu}_p &= \frac{1}{n} \sum_{j=1}^n K_b(\mathbf{X}_i^\top \bar{\boldsymbol{\theta}} - t) (\mathbf{X}_i^\top \bar{\boldsymbol{\theta}} - t)^p, \quad p = 0, 1, 2, \quad \hat{\sigma}_0^2 = \hat{\mu}_2 \hat{\mu}_0 - \hat{\mu}_1^2. \end{aligned} \quad (7)$$

Assuming that the support of $T := \mathbf{X}^\top \bar{\boldsymbol{\theta}}$, for any given unit direction $\bar{\boldsymbol{\theta}}$ is compact and is denoted by $\mathcal{T} = [0, 1]$, we partition the interval \mathcal{T} into M equal-width non-overlapping bins $\{B_1, B_2, \dots, B_M\}$, such that data belonging to different bins are independent and identically distributed. We define the mean observations $\tilde{\mathbf{X}}_l$ and \tilde{Y}_l for the data points belonging to the l -th bin, where the latter are defined as the appropriate Fréchet barycenters,

$$\tilde{\mathbf{X}}_l = \sum_{i=1}^n W_{il} \mathbf{X}_i, \quad \tilde{Y}_l = \operatorname{argmin}_{\omega \in \Omega} \sum_{i=1}^n W_{il} d^2(Y_i, \omega), \quad \text{where } W_{il} = \frac{\mathbb{I}(\mathbf{X}_i^\top \bar{\boldsymbol{\theta}} \in B_l)}{\sum_{i=1}^n \mathbb{I}(\mathbf{X}_i^\top \bar{\boldsymbol{\theta}} \in B_l)}. \quad (8)$$

Here the number of bins M depends on the sample size n . The appropriate choice of $M = M(n)$ will be discussed later. The proposed estimator for the true direction $\bar{\boldsymbol{\theta}}_0$ in (3) is then

$$\hat{\bar{\boldsymbol{\theta}}} = \operatorname{argmin}_{\bar{\boldsymbol{\theta}} \in \Theta} V_n(\bar{\boldsymbol{\theta}}), \quad \text{where } V_n(\bar{\boldsymbol{\theta}}) = \frac{1}{M} \sum_{l=1}^M d^2(\tilde{Y}_l, \hat{m}_\oplus(\tilde{\mathbf{X}}_l^\top \bar{\boldsymbol{\theta}})). \quad (9)$$

Here $\hat{m}_\oplus(\tilde{\mathbf{X}}_l^\top \bar{\boldsymbol{\theta}})$, $l = 1, \dots, M$, is the local Fréchet regression estimator, constructed based on the sample (\mathbf{X}_i, Y_i) , $i = 1, \dots, n$, and evaluated at each sample point of the binned sample $(\tilde{\mathbf{X}}_l, \tilde{Y}_l)$, $l = 1, \dots, M$, as described in (6) and (7). Define an intermediate quantity

that corresponds to the empirical version of $H(\cdot)$ in (3) as

$$\tilde{\boldsymbol{\theta}} = \underset{\bar{\boldsymbol{\theta}} \in \Theta}{\operatorname{argmin}} \tilde{V}_n(\bar{\boldsymbol{\theta}}), \text{ where } \tilde{V}_n(\bar{\boldsymbol{\theta}}) = \frac{1}{M} \sum_{l=1}^M d^2(\tilde{Y}_l, m_{\oplus}(\tilde{\mathbf{X}}_l^{\top} \bar{\boldsymbol{\theta}})). \quad (10)$$

This auxiliary quantity is used to prove the asymptotic results for $\hat{\boldsymbol{\theta}}$ in the next section.

The bandwidth $b = b(n)$ is a tuning parameter involved in the estimation and the rate of convergence for $\hat{m}_{\oplus}(\cdot)$ to $m_{\oplus}(\cdot)$ is contingent on b . It is important to note here that, another possible estimator for $m_{\oplus}(\cdot)$ could be given by the global Fréchet regression estimator introduced by Petersen and Müller (2019). This is developed by generalizing multiple linear regression to the case of a metric-valued response by viewing the regression function as a sequence of weighted Fréchet means, with weights derived from those of the corresponding standard linear regression. Using this alternative estimate for the unknown link function in the IFR model (2) avoids the tuning parameter b that is needed for local Fréchet regression.

3 Theory

The unknown quantities that constitute the Index Fréchet Regression (IFR) model consist of the nonparametric link function and the index parameter, and thus the asymptotic properties of the estimate of the true unit direction rely on those of the estimates of the link function (with local Fréchet regression) and the index parameter (through an M-estimator of the criterion function $H(\cdot)$ in (3)). The separable metric space (Ω, d) is assumed to be totally bounded with diameter D , hence separable. In addition, with regard to the quantities in (3), (6), and (9) we require the following assumptions.

- (A1) The conditional and weighted Fréchet means in (3), (4), (6) and (8) are well defined, i.e., they exist and are unique.
- (A2) The link function $m_{\oplus}(\cdot)$ is Lipschitz continuous, that is, there exists a real constant $K > 0$, such that, for all $\bar{\boldsymbol{\theta}}_1, \bar{\boldsymbol{\theta}}_2 \in \bar{\Theta}$,

$$d(m_{\oplus}(\mathbf{x}^{\top} \bar{\boldsymbol{\theta}}_1), m_{\oplus}(\mathbf{x}^{\top} \bar{\boldsymbol{\theta}}_2)) \leq K \|\mathbf{x}^{\top} (\bar{\boldsymbol{\theta}}_1 - \bar{\boldsymbol{\theta}}_2)\|.$$

- (A3) For any $\varepsilon > 0$ and $\beta_1, \beta_2 > 1$, define

$$a_n = \max\{b^{2/(\beta_1-1)}, (nb^2)^{-1/(2(\beta_2-1)+\varepsilon)}, (nb^2(-\log b)^{-1})^{1/2(\beta_2-1)}\}. \quad (11)$$

The number of non-overlapping bins defined in Section 2, M is a function of the sample

size n , that is $M = M(n)$ such that $Ma_n \rightarrow 0$.

We note that for $\beta_1 = \beta_2 = 2$, a_n reduces to

$$a_n = \max\{b^2, (nb^2)^{-1/(2+\varepsilon)}, (nb^2(-\log b)^{-1})^{1/2}\}.$$

The above assumptions are commonly imposed when one studies M-estimators. Whether Fréchet means are well defined depends on the nature of the space, as well as the metric considered. For example, in case of Euclidean responses Fréchet means coincide with the usual means for random vectors with finite second moments. For finite-dimensional Riemannian manifolds additional regularity conditions are required (Afsari, 2011; Pennec, 2018). For Hadamard spaces, unique Fréchet means are known to exist (Bhattacharya and Patrangenaru, 2003, 2005; Patrangenaru and Ellingson, 2015; Kloeckner, 2010). Assumption (A2) limits how fast the object $m_{\oplus}(\cdot)$ can change, introducing a concept of smoothness in the link function for the IFR model (2). Assumption (A1) is satisfied for the space (Ω, d_W) of univariate probability distributions with the 2-Wasserstein metric and also for the space (Ω, d_F) of covariance matrices with the Frobenius metric d_F (Dubey and Müller, 2019; Petersen and Müller, 2019). Assumption (A3) serves to connect the uniform rate of convergence a_n for the local Fréchet regression estimator as given in (11) with the number of bins M . A basic additional assumption is that the predictors needed for the nonparametric Fréchet regression are randomly distributed over the domain where the function is to be estimated, and that on average they become denser as more data are collected. This requires that there is at least one continuous predictor since if all the predictors are binary then the predictor locations cannot become denser with larger sample size. For any given direction $\bar{\theta}$, the univariate index variable $T := \mathbf{X}^\top \bar{\theta}$ is assumed to have a density $f_T(\cdot)$ with a compact support \mathcal{T} and that the multivariate random variable \mathbf{X} is bounded.

Additional assumptions (U1)-(U3), and (R1)-(R2) have been used previously in Petersen and Müller (2019) and are stated in the Appendix. They concern metric entropy and curvature for M estimators and are commonly used in their asymptotic analysis utilizing empirical process theory (Van Der Vaart and Wellner, 2000). They are specifically required to establish consistency and uniform rate of convergence for the local Fréchet regression estimator in (9) (Chen and Müller, 2020). Assumptions (R1)-(R2) are commonly used in the local regression literature (Silverman, 1978; Fan and Gijbels, 1996).

Proposition 2. *Under assumption (A1)-(A2), $H(\cdot)$ in model (3) is a continuous function of $\bar{\theta}$ and for any $\bar{\theta}_0 \in \bar{\Theta}$, $H(\bar{\theta}_0) \leq H(\bar{\theta})$.*

Most types of random objects, such as those in the Wasserstein space (the space of probability distributions equipped with the 2-Wasserstein distance) or the space of symmetric,

positive semidefinite matrices endowed with the Frobenius or power metric satisfy assumptions (U1)-(U3) (see Appendix) with $\beta_1 = \beta_2 = 2$. If one chooses the bandwidth sequence b for the local Fréchet regression such that, for a given $\varepsilon > 0$, $b \sim n^{-(\beta_1-1)/(2\beta_1+4\beta_2-6+2\varepsilon)}$, a_n is of the order $n^{-\frac{1}{(\beta_1+2\beta_2-3+\varepsilon)}}$ (Chen and Müller, 2020). For $\beta_1 = \beta_2 = 2$, this becomes $a_n \sim n^{-\frac{1}{3+\varepsilon}}$, leading to a uniform convergence rate that is arbitrarily close to $O_P(n^{-1/3})$. Any choice $M = M(n) = n^\gamma$ with $0 < \gamma < \frac{1}{3}$ will then satisfy Assumption (A3).

We will make use of the following known result to deal with the link function part when investigating the asymptotic convergence rates of the proposed IFR estimator.

Lemma 1 (Chen and Müller (2020) Theorem 1). *Under assumptions (U1)-(U3), (R1)-(R2), and if $b \rightarrow 0$, such that $nb^2(-\log b)^{-1} \rightarrow \infty$ as $n \rightarrow \infty$, for any $\varepsilon > 0$, and $\beta_1, \beta_2 > 1$ as per assumption (U3),*

$$\sup_{t \in \mathcal{T}} d(\hat{m}_\oplus(t), m_\oplus(t)) = O_P(a_n), \quad (12)$$

where a_n is as given in equation (11) in Assumption (A3).

The following result demonstrates the consistency of the proposed estimator for the true index direction. All proofs can be found in the Supplementary Material.

Theorem 1. *Under assumptions (A1)-(A2), (U1)-(U3), and (R1)-(R2),*

$$\hat{\boldsymbol{\theta}} - \bar{\boldsymbol{\theta}}_0 \xrightarrow{P} 0 \text{ on } \bar{\Theta}.$$

Any $\bar{\boldsymbol{\theta}} \in \bar{\Theta}$ is decomposed into $(\theta_1, \boldsymbol{\theta})^\top$, where $\theta_1 > 0$, and for purposes of modeling the single index, keeping identifiability in mind, can be expressed solely as a function of $\boldsymbol{\theta}$. To this end we rewrite the criteria function and the corresponding minimizers in terms of the sub-vector $\boldsymbol{\theta}$ only,

$$\boldsymbol{\theta}_0 = \underset{\boldsymbol{\theta}: \boldsymbol{\theta} \in \Theta}{\operatorname{argmin}} H(\boldsymbol{\theta}), \quad \tilde{\boldsymbol{\theta}} = \underset{\boldsymbol{\theta}: \boldsymbol{\theta} \in \Theta}{\operatorname{argmin}} \tilde{V}_n(\boldsymbol{\theta}), \quad \hat{\boldsymbol{\theta}} = \underset{\boldsymbol{\theta}: \boldsymbol{\theta} \in \Theta}{\operatorname{argmin}} V_n(\boldsymbol{\theta}). \quad (13)$$

We note that $\boldsymbol{\theta}_0$, $\tilde{\boldsymbol{\theta}}$, and $\hat{\boldsymbol{\theta}}$ are the unconstrained minimizers for the criteria functions $H(\cdot)$, $\tilde{V}_n(\cdot)$, and $V_n(\cdot)$ respectively, which are continuous functions of $\boldsymbol{\theta}$, the latter two almost surely.

Combining the consistency result for the direction vector from Theorem 1 with the uniform convergence of the local Fréchet regression estimator in Lemma 1, the asymptotic consistency of the estimated single index regression (IFR) model follows.

Corollary 1. *Under the conditions required for Theorem 1, for any $\mathbf{x} \in \mathbb{R}^p$,*

$$d(\hat{m}_\oplus(\mathbf{x}^\top \hat{\boldsymbol{\theta}}), m_\oplus(\mathbf{x}^\top \bar{\boldsymbol{\theta}}_0)) = o_P(1).$$

The above corollary justifies the effectiveness of the use of local Fréchet regression in the context of IFR.

4 Simulation studies

There are two tuning parameters involved in the implementation of the single index Fréchet regression (IFR) model in (3), namely the bandwidth $b = b(n)$ involved in the local Fréchet regression as per (2) and the number of i.i.d data points, $M = M(n)$, where the local Fréchet regression is fitted as per Assumption (A3).

The pair (b, M) can be chosen by leave-one-out cross validation, where the objective function to be minimized is the mean discrepancy between the local Fréchet regression estimates and the observed distributions for the binned data; specifically,

$$b_{opt} = \underset{(b, M)}{\operatorname{argmin}} \frac{1}{Mn} \sum_{l=1}^M \sum_{i=1}^n d^2(\tilde{Y}_l, \hat{m}_{\oplus(-i)}(\tilde{\mathbf{X}}_l^\top \bar{\boldsymbol{\theta}}))$$

where $\hat{m}_{\oplus(-i)}(\tilde{\mathbf{X}}_l^\top \bar{\boldsymbol{\theta}})$ is the local Fréchet regression estimate at $\tilde{\mathbf{X}}_l^\top \bar{\boldsymbol{\theta}}$ obtained with bandwidth b based on the sample excluding the i -th pair (\mathbf{X}_i, Y_i) , i.e.,

$$\hat{m}_{\oplus(-i)}(\tilde{\mathbf{X}}_l^\top \bar{\boldsymbol{\theta}}) = \underset{\omega \in \Omega}{\operatorname{argmin}} \frac{1}{(n-1)} \sum_{j \neq i} \hat{S}(\mathbf{X}_j^\top \bar{\boldsymbol{\theta}}, \tilde{\mathbf{X}}_l^\top \bar{\boldsymbol{\theta}}, b) d^2(Y_j, \omega),$$

In practice, we replace leave-one-out cross validation by 5-fold cross validation when $n > 30$.

The performance of the estimation is measured through simulations under various settings. The random objects we consider include samples of univariate distributions equipped with the Wasserstein-2 metric, samples of adjacency matrices from networks with the Frobenius metric and samples of multivariate data with the usual Euclidean metric. It is important to recall that true direction $\bar{\boldsymbol{\theta}}_0$ is chosen to lie on the unit sphere in \mathbb{R}^p with $\theta_{01} > 0$. In each case, the optimal direction is estimated as the minimizer of $V_n(\boldsymbol{\theta}) : \boldsymbol{\theta} \in \mathbb{R}^{p-1}$ and $\boldsymbol{\theta}^\top \boldsymbol{\theta} \leq 1$, in (9).

To evaluate the accuracy of the estimate, we repeat the data generating mechanism 500 times in each simulation setting, and for each such replication, obtain the optimal direction as $\hat{\boldsymbol{\theta}}^{(i)}$ $i = 1, \dots, 500$. The intrinsic Fréchet mean of these 500 estimates on the unit sphere is computed as $\hat{\boldsymbol{\theta}}$. Since each $\hat{\boldsymbol{\theta}}^{(i)}$ lies on the manifold (the unit sphere in \mathbb{R}^p), the bias and

deviance of the estimator is estimated as

$$\begin{aligned} \text{bias}(\widehat{\boldsymbol{\theta}}) &= \arccos\langle \widehat{\boldsymbol{\theta}}, \bar{\boldsymbol{\theta}}_0 \rangle, \\ \text{dev}(\widehat{\boldsymbol{\theta}}) &= \text{Var} \left(\arccos\langle \widehat{\boldsymbol{\theta}}^{(i)}, \widehat{\boldsymbol{\theta}} \rangle \right) \end{aligned} \quad (14)$$

Essentially, we estimate the $(p - 1)$ - dimensional parameter $\boldsymbol{\theta}_0 = (\theta_{20}, \dots, \theta_{p0})$ freely and then estimate θ_{10} from the relation $\theta_{10} = \sqrt{1 - \|\boldsymbol{\theta}_0\|^2}$.

4.1 Distributional responses

The space of distributions with the Wasserstein–2 metric provides an ideal setting for illustrating the efficacy of the proposed methods through simulation experiments. We consider distributions on a bounded domain \mathcal{T} as the response, $Y(\cdot)$, and they are represented by the respective quantile functions $Q(Y)(\cdot)$. A p - dimensional Euclidean predictor \mathbf{X} is considered. The random response is generated conditional on \mathbf{X} , by adding noise to the true regression quantile

$$Q(m_{\oplus}(\mathbf{x}))(\cdot) = \mathbb{E}(Q(Y)(\cdot) | \mathbf{X} = \mathbf{x}) \quad (15)$$

As emphasized, the conditional distribution of Y depends on \mathbf{X} only through the true index parameter $\boldsymbol{\theta}_0$. Two different simulation scenarios are examined as we generate the distribution objects from location-scale shift families (see Table 1). In the first setting, the response is generated, on average, as a normal distribution with parameters that depend on \mathbf{X} . For $\mathbf{X} = \mathbf{x}$, the distribution parameters $\mu \sim N(\zeta(\mathbf{x}^\top \boldsymbol{\theta}_0), \nu_1)$ is independently sampled, and for a fixed parameter $\sigma = 0.1$ the corresponding distribution is given by $Q(Y)(\cdot) = \mu + \sigma \Phi^{-1}(\cdot)$. Here, the relevant sub-parameter is chosen as $\nu_1 = 0.1$ and three different link functions are considered, namely $\zeta(y) = y$, $\zeta(y) = y^2$, and $\zeta(y) = \exp(y)$, and $\Phi(\cdot)$ is the standard normal distribution function. The second setting is slightly more complicated. The distributional parameter $\mu | \mathbf{X} = \mathbf{x}$ is sampled as before and $\sigma = 0.1$ is assumed to be a fixed parameter. The resulting distribution is then “transported” in Wasserstein space via a random transport map T , that is uniformly sampled from the collection of maps $T_k(a) = a - \sin(ka)/|k|$ for $k \in \{\pm 1, \pm 2, \pm 3\}$. The distributions thus generated are not Gaussian anymore due to the transportation. Nevertheless, one can show that the Fréchet mean is exactly $\mu + \sigma \Phi^{-1}(\cdot)$ as before.

To this end, we generate a random sample of size n of density objects and multivariate Euclidean predictors from the true models, incorporating measurement error as described in the two situations above. We sample the predictors \mathbf{X}_i to be of dimension $p = 4$, with

| Setting I | Setting II |
|---|---|
| $Q(Y)(\cdot) = \mu + \sigma\Phi^{-1}(\cdot)$, where $\mu \sim N(\zeta(\mathbf{x}^\top \boldsymbol{\theta}_0), \nu_1)$, $\sigma = 0.1$. | $Q(Y)(\cdot) = T\#(\mu + \sigma\Phi^{-1}(\cdot))$, where $\mu \sim N(\zeta(\mathbf{x}^\top \boldsymbol{\theta}_0), \nu_1)$, $\sigma = 0.1$, $T_k(a) = a - \sin(ka)/ a $, $k \in \{\pm 1, \pm 2, \pm 3\}$. |

Table 1: Table showing two different simulation scenarios.

the components of the vectors to be distributed independently as $Beta(1, 1)$. Three different link functions are used to simulate the densities from the “true” model, namely, the identity link, the square link, and the exponential link. The bias and deviance of the estimated direction vectors for varying sample sizes are displayed in Tables 2 and 3. We note that, the bias encountered due to the local Fréchet estimation is generally low and the variance of the estimates also diminish with a higher sample size. The performance of the fits is

| Setting I | | | | | | |
|------------|-------------------------|-------|---------------------------|-------|---------------------------|-------|
| | link1 ($x \mapsto x$) | | link2 ($x \mapsto x^2$) | | link3 ($x \mapsto e^x$) | |
| | bias | dev | bias | dev | bias | dev |
| $n = 100$ | 0.033 | 0.027 | 0.031 | 0.029 | 0.039 | 0.041 |
| $n = 1000$ | 0.011 | 0.013 | 0.017 | 0.012 | 0.020 | 0.013 |

Table 2: Table showing bias and variance of $\hat{\boldsymbol{\theta}}$ (measured in radians) based on 500 replications when the predictor dimension is $p = 4$. We took the four components of the vectors to be distributed independently as $Beta(1, 1)$. The tuning parameters (b, M) are chosen by a 5-fold cross validation method.

evaluated by computing the Mean Square Error (MSE) between the observed and the fitted distribution. Denoting the simulated true and estimated distribution objects at $(\tilde{\mathbf{X}}_l, \tilde{Y}_l)$, by $m_{\oplus}(\tilde{\mathbf{X}}_l^\top \bar{\boldsymbol{\theta}}_0)$ and $\hat{m}_{\oplus}(\tilde{\mathbf{X}}_l^\top \hat{\boldsymbol{\theta}})$ respectively, for $l = 1, \dots, M$, the utility of the estimation was measured quantitatively by

$$MSE = \frac{1}{M} \sum_{l=1}^M d_W^2(\tilde{Y}_l, \hat{m}_{\oplus}(\tilde{\mathbf{X}}_l^\top \hat{\boldsymbol{\theta}})), \quad (16)$$

where $d_W(\cdot, \cdot)$ is the Wasserstein-2 distance between two distributions. We also compared the estimation performance of the proposed single index Fréchet regression (IFR) method to a baseline Global Fréchet regression (GFR) method, which can handle multivariate predictors being a generalization of global least squares regression (Petersen and Müller, 2019). Denoting the GFR estimate of the distribution at $(\tilde{\mathbf{X}}_l, \tilde{Y}_l)$, by $\hat{g}_{\oplus}(\tilde{\mathbf{X}}_l)$ for each $l = 1, \dots, M$,

we express the MSE of the fits as

$$MSE = \frac{1}{M} \sum_{l=1}^M d_W^2(\tilde{Y}_l, \hat{g}_{\oplus}(\tilde{\mathbf{X}}_l)), \quad (17)$$

where $d_W(\cdot, \cdot)$ is the Wasserstein-2 distance between two distributions. Figure 1 shows the boxplots for different link functions used to generate the distribution data in the two simulation settings I and II for a sample size of $n = 1000$. We observe that, the IFR method outperforms the baseline GFR method in all the cases. Perhaps, the closest comparison between the two methods would be when an identity link function is used in the data generation mechanism. This is indeed expected since, in this case, the true model essentially reduces to a linear model. We also display the fitted and the true distributions represented as densities (Figure 2). The estimates from the IFR method matches the true observed densities quite well, thus the proposed IFR method can be used to validate the estimation method.

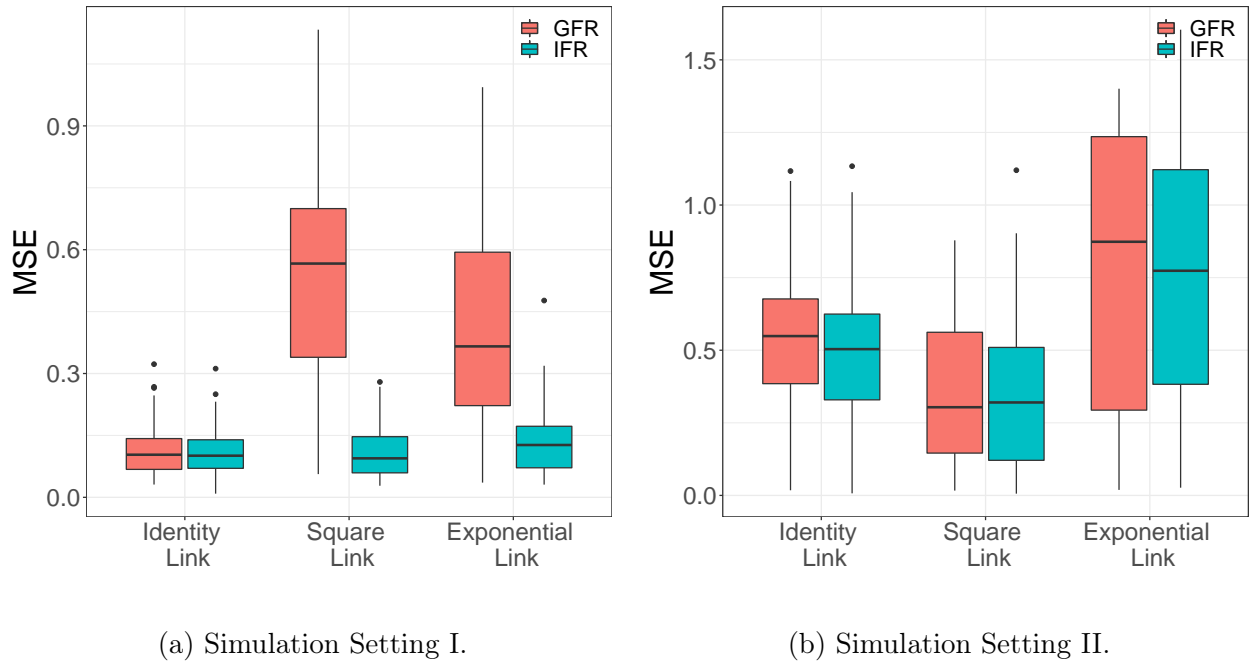


Figure 1: Boxplot of MSPE of the fits using the single index Fréchet regression model (IFR) and the Global Fréchet regression (GFR) model for a sample size $n = 1000$. The left and the right panel correspond to the simulation settings I and II, respectively. The left, middle, and right columns in each of the panels correspond to the three different link functions used in the data generation mechanism, namely, identity, square, and exponential link functions, respectively, while the link functions in all cases are estimated from the data.

| Setting II | | | | | | |
|------------|-------------------------|-------|---------------------------|-------|---------------------------|-------|
| | link1 ($x \mapsto x$) | | link2 ($x \mapsto x^2$) | | link3 ($x \mapsto e^x$) | |
| | bias | dev | bias | dev | bias | dev |
| $n = 100$ | 0.029 | 0.027 | 0.022 | 0.037 | 0.028 | 0.044 |
| $n = 1000$ | 0.010 | 0.012 | 0.011 | 0.014 | 0.017 | 0.021 |

Table 3: Table showing bias and variance of $\hat{\theta}$ (measured in radians) based on 500 replications when the predictor dimension is $p = 4$. We took the five components of the vectors to be distributed independently as $Beta(1, 1)$. The tuning parameters (b, M) are chosen by 5-fold cross validation method.

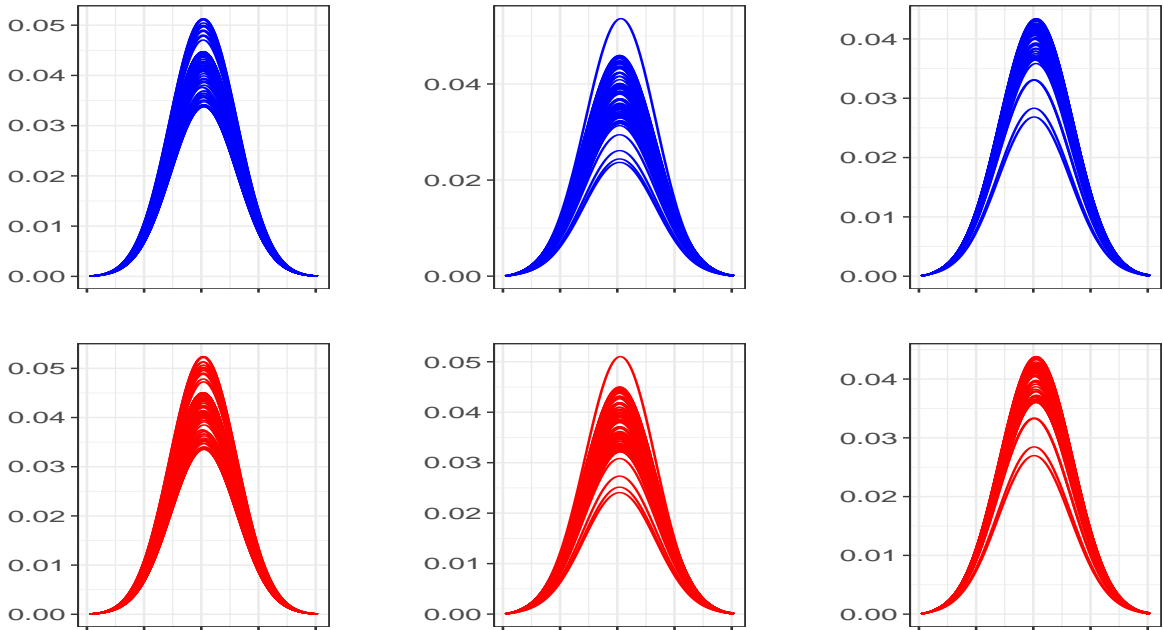


Figure 2: Figure showing the density estimates of the distribution objects generated in simulation setting I. The blue and red curves are the observed and estimated densities, respectively. The left, middle, and right panels correspond to the three different link functions used in the data generation mechanism, namely, identity, square, and exponential link functions, respectively.

4.2 Adjacency matrix responses

Here the response objects are assumed to reside in the space of adjacency matrices arising out of a weighted graph equipped with the Frobenius norm. The (p, q) -th entry of the

adjacency matrix Y is given by,

$$Y_{pq} = m(\mathbf{x}^\top \boldsymbol{\theta}_0) + \epsilon_{pq}, \quad (18)$$

where ϵ_{pq} are independently sampled errors and the link function $m(\cdot)$ is such that $Y_{pq} \in (0, 1)$ for all p, q . To ensure this, an appropriate link function in this case is taken as the expit link function, that is, $m(\mathbf{x}^\top \boldsymbol{\theta}_0) = 1/(1 + \exp(-m(\mathbf{x}^\top \boldsymbol{\theta}_0)))$. For a given index $\mathbf{x}^\top \boldsymbol{\theta}_0$, ϵ_{pq} was sampled from a Uniform distribution on $[\max\{0, -m(\mathbf{x}^\top \boldsymbol{\theta}_0)\}, \min\{1, 1 - m(\mathbf{x}^\top \boldsymbol{\theta}_0)\}]$. We generated

| | link ($x \mapsto 1/(1 + \exp(-x))$) | |
|------------|---------------------------------------|-------|
| | bias | dev |
| $n = 100$ | 0.044 | 0.052 |
| $n = 1000$ | 0.021 | 0.019 |

Table 4: Table showing bias and variance of $\hat{\theta}$ (measured in radians) based on 500 replications for weighted adjacency matrix responses. The tuning parameters for the model-fitting are chosen by 5– fold cross validation method.

samples of networks with 10 nodes, as one might encounter in brain networks, with the weighted adjacency computed as per (18). The predictors are sampled from a 4–dimensional multivariate normal distributions, where each of the components was truncated to lie between $[-5, 5]$. While the mean vector for the multivariate normal distribution in the data generation scheme is assumed to be the zero vector, we assume the associated covariance matrix to be non-identity with $\text{cor}(X_1, X_2) = \text{cor}(X_1, X_3) = \text{cor}(X_2, X_3) = 0.3$, and $\text{cor}(X_1, X_4) = \text{cor}(X_2, X_4) = -0.4$. The variances for each of the four components are assumed equal to 0.25. We note here that the non-zero correlation among the components of the predictor vector does not influence the performance of the nonparametric regression fit negatively. Table 4 presents the bias and variance of the estimator computed based on 500 replication of the data generating process.

4.3 Euclidean responses

Here the object response of interest is assumed to lie in the Euclidean space. For generating the predictor vectors we consider a 5–dimensional vector distributed as truncated multivariate normal distributions, where each of the components is truncated to lie between $[-10, 10]$. The components are assumed to be correlated such that X_1 correlates with X_2 and X_3 with $r = 0.5$, and X_2 and X_3 correlate with $r = 0.25$. The variances for each of the five components are 0.1. The consistency of the estimates is illustrated in Table 5 based on 500 replications of the simulation scenario.

| | link1 ($x \mapsto x$) | | link2 ($x \mapsto x^2$) | | link3 ($x \mapsto e^x$) | |
|------------|-------------------------|-------|---------------------------|-------|---------------------------|-------|
| | bias | dev | bias | dev | bias | dev |
| $n = 100$ | 0.013 | 0.061 | 0.025 | 0.048 | 0.037 | 0.029 |
| $n = 1000$ | 0.006 | 0.021 | 0.014 | 0.019 | 0.013 | 0.009 |

Table 5: Table showing bias and variance of $\hat{\theta}$ (measured in radians) based on 500 replications for a Euclidean vector response. The predictors X_1, \dots, X_5 are generated from a truncated multivariate normal distribution.

5 Data analysis

Modern functional Magnetic Resonance Imaging (fMRI) methodology has made it possible to study structural elements of the brain and identify brain regions or cortical hubs that exhibit similar behavior, especially when subjects are in the resting state (Allen et al., 2014; Ferreira and Busatto, 2013). In resting state fMRI, a time series of Blood Oxygen Level Dependent (BOLD) signal is observed for the seed voxels in selected functional hubs. For each hub, a seed voxel is identified as the voxel whose signal has the highest correlation with the signals of nearby voxels. Alzheimer’s Disease has been found to have associations with anomalies in functional integration of brain regions and target regions or hubs of high connectivity in the brain (Damoiseaux et al., 2012; Zhang et al., 2010).

Data used in the preparation of this article were obtained from the Alzheimer’s Disease Neuro-imaging Initiative (ADNI) database (adni.loni.usc.edu). BOLD signals for $V = 11$ brain seed voxels for each subject were extracted. These Regions of Interest are aMPFC (Anterior medial prefrontal cortex), PCC (Posterior cingulate cortex), dMFPC (Dorsal medial prefrontal cortex), TPJ (Temporal parietal junction), LTC (Lateral temporal cortex), TempP (Temporal pole), vMFPC (Ventral medial prefrontal cortex), pIPL (Posterior inferior parietal lobule), Rsp (Retrosplenial cortex), PHC (Parahippocampal cortex), and HF⁺ (Hippocampal formation) (Andrews-Hanna et al., 2010). The pre-processing of the BOLD signals was implemented by adopting the standard procedures of slice-timing correction, head motion correction and normalization and other standard steps. The signals for each subject were recorded over the interval $[0, 270]$ (in seconds), with $K = 136$ measurements available at 2 second intervals. From this the temporal correlations were computed to construct the connectivity correlation matrix, also referred to as the Pearson correlation matrix in the area of fMRI studies.

The data set in our analysis consists of $n = 830$ subjects at the four stages of the disease: 372 CN (cognitively normal), 113 EMCI (early mild cognitive impairment), 200 LMCI (late mild cognitive impairment), and 145 AD subjects were considered. The inter-

hub connectivity Pearson correlation matrix for the $i - th$ subject is denoted as Y_i , and has the (q, r) -th element

$$(Y_i)_{qr} = \frac{\sum_{p=1}^K (s_{ipq} - \bar{s}_{iq})(s_{ipr} - \bar{s}_{ir})}{\left[\left(\sum_{p=1}^K (s_{ipq} - \bar{s}_{iq})^2 \right) \left(\sum_{p=1}^K (s_{ipr} - \bar{s}_{ir})^2 \right) \right]^{1/2}}, \quad (19)$$

where s_{ipq} is the (p, q) th element of the signal matrix for the i th subject and $\bar{s}_{iq} := \frac{1}{K} \sum_{p=1}^K s_{ipq}$ is the mean signal strength for the q th voxel. For Alzheimer’s disease trials, ADAS-Cog-13 is a widely-used measure of cognitive performance. It measures impairments across several cognitive domains that are considered to be affected early and characteristically in Alzheimer’s disease (Rockwood et al., 2007; Kueper et al., 2018). It is important to note that higher scores are associated with more serious cognitive deficiency.

To demonstrate the validity of the model, we consider the out-of-sample prediction performance of the proposed IFR. For this, we first randomly split the dataset into a training set with sample size n_{train} and a test set with the remaining n_{test} subjects. The IFR method was implemented as follows - for any given unit direction $\bar{\boldsymbol{\theta}} \in \bar{\Theta}$, we partition the domain of the projections into M equal-width non-overlapping bins and compute the mean observations $\tilde{\mathbf{X}}_l$ and \tilde{Y}_l for the data points belonging to the l -th bin, where the latter are defined as the appropriate Fréchet barycenters. Observe that M is dependent on the sample size. The “true” index is estimated as $\hat{\boldsymbol{\theta}}$ as per (9). We then take the fitted objects obtained from the training set, and predict the responses in the test set using the covariates present in the test set. As a measure of the efficacy of the fitted model, we compute root mean squared prediction error (RMPE) as

$$\text{RMPE} = \left[\frac{1}{M_{n_{\text{test}}}} \sum_{i=1}^{M_{n_{\text{test}}}} d_F^2 \left(\tilde{Y}_l^{\text{test}}, \hat{m}_{\oplus}(\tilde{\mathbf{X}}_l^{\top} \hat{\boldsymbol{\theta}}) \right) \right]^{-1/2}, \quad (20)$$

where $\tilde{Y}_l^{\text{test}}$ and $\hat{m}_{\oplus}(\tilde{\mathbf{X}}_l^{\top} \hat{\boldsymbol{\theta}})$ denote, respectively, the l th observed and predicted responses in the test set, evaluated at the binned average $\tilde{\mathbf{X}}_l$. We repeat this process 500 times, and compute RMPE for each split for the subjects separately (See Table 6). The tuning parameters (b, M) are chosen by a 5-fold cross validation method for each replication of the process. We observe that the out-of-sample predictions error is quite low for after fitting the IFR model. In fact it is very close to the in-sample-prediction error (0.251), calculated as the average distance between the observed training sample and the predicted objects based on the covariates in the training sets, which supports the validity of the proposed IFR models.

Another interest of our study was to understand the effect of various relevant predictors,

| n_{train} | n_{test} | RMPE for the IFR method |
|--------------------|-------------------|-------------------------|
| 500 | 330 | 0.206 |

Table 6: Average Root Mean Prediction Error (RMPE) over 1000 repetitions for the subjects, as obtained from the local fits of the single Index Fréchet Regression (IFR) model. Here, n_{train} and n_{test} denote the sample sizes for the split training and testing datasets respectively.

such as age, gender, total score, and stage of the disease on the inter-hub functional connectivity. In particular, the hypothesis to test is given by $H_0 : m_{\oplus}(\cdot) = m_{\oplus}(\theta_1 X_1)$ vs. $H_1 : m_{\oplus}(\cdot) = m_{\oplus}(\sum_{j=1}^p \theta_j X_j)$, or equivalently

$$H_0 : \boldsymbol{\theta} = \mathbf{0}_{(p-1) \times 1} \text{ vs. } H_1 : \text{not all } \theta_j \text{ are } 0, j = 2, \dots, p$$

where $\bar{\boldsymbol{\theta}} = (\theta_1, \boldsymbol{\theta})^\top$ and $\boldsymbol{\theta} = (\theta_2, \dots, \theta_p)$. Here we consider $p = 10$, predictors, namely, $X_1 =$ stages for the disease, $X_2 =$ age, $X_3 =$ sex, $X_4 =$ total ADAS score, and the pairwise interaction terms between them as $X_5 = X_1 X_2$, $X_6 = X_1 X_3$, $X_7 = X_1 X_4$, $X_8 = X_2 X_3$, $X_9 = X_2 X_4$, and $X_{10} = X_3 X_4$.

We employ a bootstrap procedure to test for H_0 . Based on a standard bootstrap approach, we resample (\mathbf{X}_i^*, Y_i^*) a large number of times, B . For each of these B bootstrap samples, the estimated direction as $\hat{\boldsymbol{\theta}}^*$ ($(p-1)$ -dimensional vector) is computed. We estimate the full p -dimensional vector $\hat{\boldsymbol{\theta}}^*$ for each of the bootstrap sample, where $\hat{\boldsymbol{\theta}}^* = (\hat{\theta}_1^*, \hat{\boldsymbol{\theta}}^*)$, with $\hat{\theta}_1^* = \sqrt{1 - \|\hat{\boldsymbol{\theta}}^*\|^2}$. Denote the p -dimensional unit vector estimated from the original sample as $\hat{\boldsymbol{\theta}}$. $\hat{\boldsymbol{\theta}}$ and $\hat{\boldsymbol{\theta}}^*$ for all B bootstrap samples, lie on a sphere in \mathbb{R}^p . We can compute the geodesic distance between two points $\bar{\boldsymbol{\gamma}}_1$ and $\bar{\boldsymbol{\gamma}}_2$ situated on the boundary of a unit sphere by $d_g(\bar{\boldsymbol{\gamma}}_1, \bar{\boldsymbol{\gamma}}_2) = \arccos\langle \bar{\boldsymbol{\gamma}}_1, \bar{\boldsymbol{\gamma}}_2 \rangle$. To this end, we proceed to conduct a bootstrap test as follows.

1. Compute $d_g(\hat{\boldsymbol{\theta}}^{*(b)}, \bar{\boldsymbol{\theta}}_0)$, where $\hat{\boldsymbol{\theta}}^{*(b)}$ is the p -dimensional unit vector estimated based on the b -th bootstrap sample, $b = 1, \dots, B$ and $\bar{\boldsymbol{\theta}}_0 = (1, 0, \dots)_{p \times 1}$.
2. The Achieved Significance Level (ASL) of the bootstrap test is given by

$$ASL = \frac{1}{B} \sum_{b=1}^B d_g(\hat{\boldsymbol{\theta}}^{*(b)}, \bar{\boldsymbol{\theta}}_0) > d_g(\hat{\boldsymbol{\theta}}, \hat{\boldsymbol{\theta}}^{*(b)}),$$

3. If $ASL < \alpha$ reject the null hypothesis at level α .

We carried out the procedure for testing the significance of the other predictors when “stages of the disease” is assumed to be included in the model. The ASL for the bootstrap test came

out to be 0.012, thus giving evidence for rejecting H_0 at level $\alpha = 0.05$. That is, not all of the $(p - 1)$ predictors are insignificant.

| | Step 1 | | Step 2 | | Step 3 | |
|-------------|--------|-------|--------|-------|--------|-------|
| | Coeff. | ASL | Coeff. | ASL | Coeff | ASL |
| Age | -0.364 | 0.005 | -0.394 | - | -0.401 | - |
| Gender | 0.371 | 0.122 | 0.558 | 0.161 | 0.279 | 0.113 |
| Total Score | 0.198 | 0.094 | 0.207 | 0.010 | 0.173 | - |

Table 7: Table shows the coefficients and p-values for the step-wise addition of predictors to quantify their relative significance.

We further performed a sequential addition of predictors to quantify their relative significance. For this, we specify an “alpha-to-enter” significance level at $\alpha = 0.05$ and fit each of the one-predictor model. To this end, we consider X_1 to be in the model and fit model (3) to estimate the direction index. In particular, we include each of X_2 , X_3 , and X_4 in the model along with X_1 and test whether the corresponding effect is significant, i.e., we test $\theta_j = 0$, $j = 2, 3, 4$ separately. The first predictor to be included in the step-wise model is the predictor that has the smallest *ASL*. We stop if no predictor has a test *ASL* less than α . Table 7 illustrates the step-wise addition of predictors for all one-predictor models. The first predictor to be added at level 0.05, when X_1 (“stage of the disease”) is already in the model, is X_2 (age). Interestingly, a negative value of $\hat{\theta}_2$ (-0.364) signifies a possible negative effect of the predictor on the response. This is quite expected since Alzheimer’s is a disease that is known to progress with age. In step 2, X_4 (total score) is added as a significant predictor at 0.05 level. Here the estimate $\hat{\theta}_4 = 0.207$ can be interpreted as the possible association of a higher value of the total score with greater cognitive impairment. The effect of X_3 (gender) is deemed not significant.

Finally, with X_1 , X_2 , and X_4 in the model, we test for significance of the pairwise interactions terms. The hypothesis of interest is $H_0 : \theta_5 = \theta_6 = \dots = \theta_{10} = 0$. The *ASL* for the test comes out to be 0.106, giving evidence for no significant pairwise interaction to be included in the model. Thus we estimate the relevant “true” model in this case as $E_{\oplus}(Y|\mathbf{X}^T\boldsymbol{\theta}) = m_{\oplus}(X_1\theta_1 + X_2\theta_2 + X_4\theta_4)$. The estimated average Fréchet error $\frac{1}{n} \sum_{i=1}^n d^2(Y_i, \hat{m}_{\oplus}(X_{1i}\hat{\theta}_1 + X_{2i}\hat{\theta}_2 + X_{4i}\hat{\theta}_4))$ is quite small (0.239).

To demonstrate the validity of the IFR method, we compute the estimated indices for the final model as $X_1\hat{\theta}_1 + X_2\hat{\theta}_2 + X_4\hat{\theta}_4$, for each subject and calculate the 25%, 50%, and 75% quantiles of the index. These come out to be $q_1 = 15.048$, $q_2 = 16.430$, and $q_3 = 18.250$, respectively. We find the subjects who have their estimated index values closest to q_1 , q_2 , and q_3 respectively. Table 8 shows the details on the three subjects selected. We

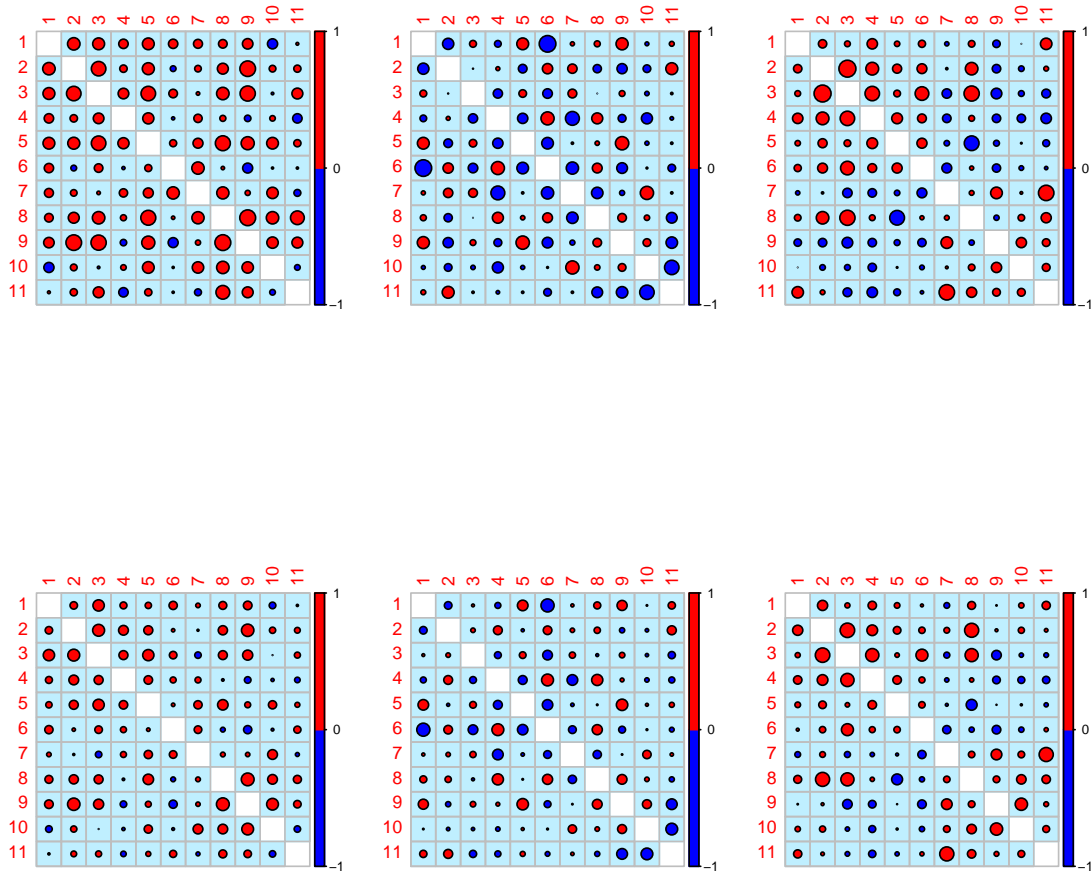


Figure 3: The observed and fitted functional connectivity matrices for an increasing value of the single index are plotted. The estimated direction $\hat{\theta}$ is computed for the final model, and the estimated index $\mathbf{X}_i^T \hat{\theta}$ are calculated. The panels in the top row, from left to right, depict the observed functional connectivity correlation matrices for the subjects, for whom the estimated index values are the closest to the 25%, 50%, and 75% of the estimated index respectively. The bottom row shows the fitted functional connectivity correlation matrices for the same subjects, the link functions estimated using the nonparametric Fréchet regression at the given quantiles (from left to right). Positive (negative) values are drawn in red (blue) and larger circles correspond to larger absolute values. The figure illustrates the dependence of functional connectivity on the overall index effect.

compare the observed and fitted functional connectivity correlation matrices for these three subjects, where the object link function is fitted by the local Fréchet regression method at the

| Subject number | Estd. index value | Stage of the disease | Age | Gender | Total score |
|----------------|-------------------|----------------------|---------|--------|-------------|
| 726 | 15.045 | 2 | 66.10 y | M | 20.33 |
| 695 | 16.430 | 2 | 78.12 y | M | 14 |
| 556 | 18.252 | 1 | 72.55 y | M | 51.67 |

Table 8: Table showing the details on the subjects who have their estimated index values closest to the first three quantiles of the estimated index, $q_1(15.048)$, $q_2(16.430)$, and $q_3(18.250)$, respectively. The subject number 726 has his estimated index value closest to q_1 and so on.

estimated index values corresponding to each subject. This gives an intuitive idea of how the estimated link function at the estimated direction vector given by $\hat{m}_{\oplus}(\mathbf{x}^T \hat{\boldsymbol{\theta}})$ changes with an increasing value of the index $\mathbf{x}^T \hat{\boldsymbol{\theta}}$, and thus brings about the effectiveness of the IFR model. In Figure 3 we display the observed (top row) and fitted (bottom row) correlation matrices for an increasing value of the single index at q_1 , q_2 , and q_3 respectively, in the columns from left to right. We observe that the fits match the general pattern of the observed matrices quite well. Indeed the Frobenius distance between the observed and the estimated matrices at q_1 , q_2 , and q_3 are calculated as 1.68, 1.10, and 0.79, respectively. A seeming tendency to have more negative correlation values in the connectivity matrices with increasing index values is an interesting finding. An overall effect of stages of the disease, age, and total score tends to influence the connectivity pattern in the brain of the Alzheimer’s patients. A higher index value would imply more cognitive deficiency in this case, which matches the widely held beliefs.

6 Discussion

The proposed single Index Fréchet Regression (IFR) model provides a new tool for the regression analysis of random object data, which are increasingly encountered in modern data analysis. Instead of a two step procedure to estimate the link function and the index parameter separately, we discuss a direct M-estimation approach. In fact, the proposed method is a combination of multivariate M-estimation (for the index vector) and Fréchet regression (for the link function) that extends the regression regime to object data responses. The index parameter is recovered as the unit direction minimizing the “residual sum of squares” after fitting the Fréchet model. In fact, any other convex loss function can be used for this purpose. For an efficient computation, we use the *Julia* language and parallel programming to estimate the minimizer direction $\hat{\boldsymbol{\theta}}$ by searching over 1000 directions such that the Fréchet variance is minimized. In a 25 core computing system, for a sample size

$n = 1000$, determining the optimal direction takes about 2 hours, while employing a 5-fold cross validation method to select the tuning parameters (b, M) .

In this project, we provide the asymptotic results involving the estimation of the index parameter which could be extended for inference. In particular, single index models being a generalization of linear regression, the interpretability of the index parameter is important for testing the effect of a subset of predictors in modulating the response. The same is true in our IFR model, despite the responses being situated in a general metric space, as illustrated by the fMRI brain imaging example.

Appendix

A.1. Technical assumptions regarding local Fréchet regression

Recall, for any given direction $\boldsymbol{\theta}$, such that $\mathbf{x}^\top \boldsymbol{\theta} = t$, the conditional Fréchet mean is given by

$$m_{\oplus}(t) = \operatorname{argmin}_{\omega \in \Omega} M(\omega, t); \quad M(\omega, t) := \mathbb{E}(d^2(Y, \omega) | \mathbf{X}^\top \boldsymbol{\theta} = t). \quad (21)$$

The local Fréchet regression estimate is given by

$$\hat{m}_{\oplus}(t) = \operatorname{argmin}_{\omega \in \Omega} \hat{L}_n(\omega, t); \quad \hat{L}_n(\omega, t) := \frac{1}{n} \sum_{i=1}^n \hat{S}(\mathbf{X}_i^\top \boldsymbol{\theta}_1, t, h) d^2(Y_i, \omega). \quad (22)$$

Let us define the intermediate localized weighted Fréchet mean as

$$\tilde{m}_{\oplus}(t) = \operatorname{argmin}_{\omega \in \Omega} \tilde{L}_b(\omega, t); \quad \tilde{L}_b(\omega, t) := \mathbb{E}(S(\mathbf{X}^\top \boldsymbol{\theta}_1, t, h) d^2(Y, \omega)). \quad (23)$$

The marginal density f_T of $T := \mathbf{X}^\top \boldsymbol{\theta}$, for any $\boldsymbol{\theta} \in \mathbb{R}^{p-1}$ and $\boldsymbol{\theta}^\top \boldsymbol{\theta} \leq 1$, is bounded away from zero on its support \mathcal{T} , i.e., $\inf_{t \in \mathcal{T}} f_T(t) > 0$. We require the following assumptions for as described in [Chen and Müller \(2020\)](#).

(U1) For all $t \in \mathcal{T}$, the minimizers $m_{\oplus}(t)$, $\hat{m}_{\oplus}(t)$, and $\tilde{m}_{\oplus}(t)$ exist and are unique, the latter two almost surely. In addition, for any $\varepsilon > 0$,

$$\begin{aligned} & \inf_{t \in \mathcal{T}} \inf_{d(m_{\oplus}(t), \omega) > \varepsilon} [M(\omega, t) - M(m_{\oplus}(t), t)] > 0, \\ & \liminf_{b \rightarrow 0} \inf_{t \in \mathcal{T}} \inf_{d(\omega, \tilde{m}_{\oplus}(t)) > \varepsilon} [\tilde{L}_b(\omega, t) - \tilde{L}_b(\tilde{m}_{\oplus}(t), t)] > 0, \end{aligned} \quad (24)$$

and there exists $c = c(\varepsilon) > 0$ such that

$$P \left(\inf_{t \in \mathcal{T}} \inf_{d(\hat{m}_\oplus(t), \omega) > \varepsilon} [\hat{L}_n(\omega, t) - \hat{L}_n(\hat{m}_\oplus(t), t)] \geq c \right) \rightarrow 1. \quad (25)$$

(U2) Let $\mathcal{B}_r(m_\oplus(t)) \subset \Omega$ be a ball of radius r centered at $m_\oplus(t)$ and $\mathcal{N}(\varepsilon, \mathcal{B}_r(m_\oplus(t)), d)$ be its covering number using balls of radius ε . Then

$$\lim_{r \rightarrow 0^+} \int_0^1 \sup_{t \in \mathcal{T}} \sqrt{1 + \log \mathcal{N}(r\varepsilon, \mathcal{B}_r(m_\oplus(t)), d)} d\varepsilon = O(1). \quad (26)$$

(U3) There exists $r_1, r_2 > 0$, $c_1, c_2 > 0$, and $\beta_1, \beta_2 > 1$ such that

$$\begin{aligned} \inf_{t \in \mathcal{T}} \inf_{d(m_\oplus(t), \omega) < r_1} [M(\omega, t) - M(m_\oplus(t), t) - c_1 d^2(\omega, m_\oplus(t))^{\beta_1}] &\geq 0, \\ \liminf_{b \rightarrow 0} \inf_{t \in \mathcal{T}} \inf_{d(\tilde{m}_\oplus(t), \omega) < r_2} [\tilde{L}_b(\omega, t) - \tilde{L}_b(d(\tilde{m}_\oplus(t), t) - c_2 d^2(\omega, \tilde{m}_\oplus(t))^{\beta_2})] &\geq 0. \end{aligned} \quad (27)$$

Furthermore, we require the following assumptions.

(R1) The kernel K is a probability density function, symmetric around zero, uniformly continuous on \mathbb{R} such that $\int_{\mathbb{R}} K(x)^j x^k < \infty$, for $r, s = 1, \dots, 6$. The derivative K' exists and is bounded on the support of K , i.e., $\sup_{x: K(x) > 0} |K'(x)| < \infty$. Additionally, $\int_{\mathbb{R}} x^2 |K'(x)| \sqrt{|x \log |x||} dx < \infty$.

(R2) The marginal density f_T of $T = \mathbf{X}^\top \boldsymbol{\theta}$ for any given unit direction $\boldsymbol{\theta}$ and the conditional densities $f_{T|Y}(\cdot, y)$ of $T = \mathbf{X}^\top \boldsymbol{\theta}$ given $Y = y$ exist and are twice continuously differentiable on the interior of \mathcal{T} , the latter for all $y \in \Omega$. The marginal density f_T is bounded away from zero on its support \mathcal{T} , i.e., $\inf_{t \in \mathcal{T}} f_T(t) > 0$. The second-order derivative f_T'' is uniformly bounded, $\sup_{\mathcal{T}} |f_T''(t)| < \infty$. The second-order partial derivatives $(\partial^2 f_{T|Y} / \partial t^2)(\cdot, y)$ are uniformly bounded, $\sup_{y, t} |(\partial^2 f_{T|Y} / \partial t^2)(\cdot, y)| < \infty$. Additionally, for any open set $U \subset \Omega$, $P(Y \in U | T = t)$ is continuous as a function of t .

References

- Afsari, B. (2011). Riemannian L^p center of mass: existence, uniqueness, and convexity. *Proceedings of the American Mathematical Society*, 139(2):655–673.
- Allen, E., Damaraju, E., Plis, S., Erhardt, E., Eichele, T., and Calhoun, V. (2014). Tracking whole-brain connectivity dynamics in the resting state. *Cerebral Cortex*, 24(3):663–676.

- Andrews-Hanna, J. R., Reidler, J. S., Sepulcre, J., Poulin, R., and Buckner, R. L. (2010). Functional-anatomic fractionation of the brain’s default network. *Neuron*, 65(4):550–562.
- Bhattacharya, R. and Patrangenaru, V. (2003). Large sample theory of intrinsic and extrinsic sample means on manifolds. *The Annals of Statistics*, 31(1):1–29.
- Bhattacharya, R. and Patrangenaru, V. (2005). Large sample theory of intrinsic and extrinsic sample means on manifolds:II. *The Annals of Statistics*, 33(3):1225–1259.
- Carroll, R. J., Fan, J., Gijbels, I., and Wand, M. P. (1997). Generalized partially linear single-index models. *Journal of the American Statistical Association*, 92(438):477–489.
- Chang, Z., Xue, L., and Zhu, L. (2010). On an asymptotically more efficient estimation of the single-index model. *Journal of Multivariate Analysis*, 101(8):1898–1901.
- Chen, C.-H. and Li, K.-C. (1998). Can SIR be as popular as multiple linear regression? *Statistica Sinica*, 8(2):289–316.
- Chen, D., Hall, P., and Müller, H.-G. (2011). Single and multiple index functional regression models with nonparametric link. *The Annals of Statistics*, 39(3):1720–1747.
- Chen, Y. and Müller, H.-G. (2018). Wasserstein gradients for the temporal evolution of probability distributions. *arXiv preprint arXiv:1809.03498*.
- Chen, Y. and Müller, H.-G. (2020). Uniform convergence of local fréchet regression, with applications to locating extrema and time warping for metric-space valued trajectories. *arXiv: Methodology*.
- Cook, R. D. (1994). Using dimension-reduction subspaces to identify important inputs in models of physical systems. In *Proceedings of the Section on Physical and Engineering Sciences*, pages 18–25.
- Cook, R. D. and Weisberg, S. (1991). Discussion of sliced inverse regression for dimension reduction. *Journal of the American Statistical Association*, 86(414):328–332.
- Cui, X., Härdle, W. K., and Zhu, L. (2011). The EFM approach for single-index models. *The Annals of Statistics*, 39(3):1658–1688.
- Damoiseaux, J. S., Prater, K. E., Miller, B. L., and Greicius, M. D. (2012). Functional connectivity tracks clinical deterioration in Alzheimer’s disease. *Neurobiology of Aging*, 33(4):828.
- Delicado, P. and Vieu, P. (2017). Choosing the most relevant level sets for depicting a sample of densities. *Computational Statistics*, 32(3):1083–1113.
- Dubey, P. and Müller, H.-G. (2019). Fréchet analysis of variance for random objects. *Biometrika*, 106(4):803–821.
- Fan, J. and Gijbels, I. (1996). *Local Polynomial Modelling and Its Applications: Monographs on Statistics and Applied Probability 66*. Chapman & Hall/CRC.

- Fan, Y. (1995). Average derivative estimation with errors-in-variables. *Journal of Nonparametric Statistics*, 4(4):395–407.
- Ferraty, F., Park, J., and Vieu, P. (2011). Estimation of a functional single index model. In *Recent Advances in Functional Data Analysis and Related Topics*, pages 111–116. Springer.
- Ferreira, L. R. K. and Busatto, G. F. (2013). Resting-state functional connectivity in normal brain aging. *Neuroscience & Biobehavioral Reviews*, 37(3):384–400.
- Fréchet, M. R. (1948). Les éléments aléatoires de nature quelconque dans un espace distancié. *Annales de l'institut Henri Poincaré*, 10(4):215–310.
- Friedman, J. H. and Stuetzle, W. (1981). Projection pursuit regression. *Journal of the American Statistical Association*, 76(376):817–823.
- González-Briones, A., Villarrubia, G., Paz, J. F. D., and Corchado, J. (2018). A multi-agent system for the classification of gender and age from images. *Comput. Vis. Image Underst.*, 172:98–106.
- Hall, P. (1989). On projection pursuit regression. *The Annals of Statistics*, 17(2):573–588.
- Härdle, W., Hall, P., and Ichimura, H. (1993). Optimal smoothing in single-index models. *The Annals of Statistics*, 28(1):157–178.
- Härdle, W. and Stoker, T. M. (1989). Investigating smooth multiple regression by the method of average derivatives. *Journal of the American Statistical Association*, 84(408):986–995.
- Heckman, N. E. (1986). Spline smoothing in a partly linear model. *Journal of the Royal Statistical Society: Series B (Methodological)*, 48(2):244–248.
- Hristache, M., Juditsky, A., and Spokoiny, V. (2001). Direct estimation of the index coefficient in a single-index model. *The Annals of Statistics*, 29(3):595–623.
- Huh, J. and Park, B. (2002). Likelihood-based local polynomial fitting for single-index models. *Journal of Multivariate Analysis*, 80(2):302–321.
- Ichimura, H. (1993). Semiparametric least squares (SLS) and weighted SLS estimation of single-index models. *Journal of Econometrics*, 58(1-2):71–120.
- Jiang, C.-R. and Wang, J.-L. (2011). Functional single index models for longitudinal data. *The Annals of Statistics*, 39(1):362–388.
- Kereta, Ž., Klock, T., and Naumova, V. (2020). Nonlinear generalization of the monotone single index model. *Information and Inference: A Journal of the IMA*.
- Kloeckner, B. (2010). A geometric study of Wasserstein spaces: Euclidean spaces. *Annali della Scuola Normale Superiore di Pisa-Classe di Scienze*, 9(2):297–323.
- Kuchibhotla, A. K. and Patra, R. K. (2020). Efficient estimation in single index models through smoothing splines. *Bernoulli*, 26(2):1587 – 1618.

- Kuchibhotla, A. K., Patra, R. K., and Sen, B. (2017). Efficient estimation in convex single index models. *arXiv preprint arXiv:1708.00145*.
- Kueper, J. K., Speechley, M., and Montero-Odasso, M. (2018). The Alzheimer’s disease assessment scale–cognitive subscale (adas-cog): modifications and responsiveness in pre-dementia populations. a narrative review. *Journal of Alzheimer’s Disease*, 63(2):423–444.
- Li, B. and Wang, S. (2007). On directional regression for dimension reduction. *Journal of the American Statistical Association*, 102(479):997–1008.
- Li, K.-C. (1991). Sliced inverse regression for dimension reduction. *Journal of the American Statistical Association*, 86(414):316–327.
- Li, K.-C. and Duan, N. (1989). Regression analysis under link violation. *The Annals of Statistics*, 17(1):1009–1052.
- Liang, H., Liu, X., Li, R., and Tsai, C.-L. (2010). Estimation and testing for partially linear single-index models. *The Annals of Statistics*, 38(6):3811.
- Lin, W. and Kulasekera, K. (2007). Identifiability of single-index models and additive-index models. *Biometrika*, 94(2):496–501.
- Marron, J. S. and Alonso, A. M. (2014). Overview of object oriented data analysis. *Biometrical Journal*, 56(5):732–753.
- Müller, H.-G. (2016). Peter Hall, functional data analysis and random objects. *The Annals of Statistics*, 44(5):1867–1887.
- Novo, S., Aneiros, G., and Vieu, P. (2019). Automatic and location-adaptive estimation in functional single-index regression. *Journal of Nonparametric Statistics*, 31(2):364–392.
- Patrangenaru, V. and Ellingson, L. (2015). *Nonparametric Statistics On Manifolds And Their Applications To Object Data Analysis*. CRC Press.
- Pennec, X. (2018). Barycentric subspace analysis on manifolds. *The Annals of Statistics*, 46(6A):2711–2746.
- Petersen, A., Deoni, S., and Müller, H.-G. (2019). Fréchet estimation of time-varying covariance matrices from sparse data, with application to the regional co-evolution of myelination in the developing brain. *The Annals of Applied Statistics*, 13(1):393–419.
- Petersen, A. and Müller, H.-G. (2019). Fréchet regression for random objects with Euclidean predictors. *The Annals of Statistics*, 47(2):691–719.
- Peyré, G. (2009). Manifold models for signals and images. *Computer Vision and Image Understanding*, 113(2):249–260.
- Powell, J. L., Stock, J. H., and Stoker, T. M. (1986). Semiparametric estimation of weighted average derivatives. Working papers 1793-86., Massachusetts Institute of Technology (MIT), Sloan School of Management.

- Rice, J. (1986). Convergence rates for partially splined models. *Statistics & Probability Letters*, 4(4):203–208.
- Rockwood, K., Fay, S., Gorman, M., Carver, D., and Graham, J. E. (2007). The clinical meaningfulness of adas-cog changes in Alzheimer’s disease patients treated with donepezil in an open-label trial. *BMC Neurology*, 7(1):1–8.
- Ruppert, D., Wand, M. P., and Carroll, R. J. (2003). *Semiparametric Regression*. Number 12. Cambridge university press.
- Silverman, B. W. (1978). Weak and Strong Uniform Consistency of the Kernel Estimate of a Density and its Derivatives. *The Annals of Statistics*, 6(1):177 – 184.
- Small, C. G. (2012). *The Statistical Theory of Shape*. Springer Science & Business Media.
- Stoker, T. M. (1986). Consistent estimation of scaled coefficients. *Econometrica: Journal of the Econometric Society*, 54(6):1461–1481.
- Thomas Yeo, B., Krienen, F. M., Sepulcre, J., Sabuncu, M. R., Lashkari, D., Hollinshead, M., Roffman, J. L., Smoller, J. W., Zöllei, L., Polimeni, J. R., et al. (2011). The organization of the human cerebral cortex estimated by intrinsic functional connectivity. *Journal of Neurophysiology*, 106(3):1125–1165.
- Tsochantaridis, I., Hofmann, T., Joachims, T., and Altun, Y. (2004). Support vector machine learning for interdependent and structured output spaces. In *Proceedings of the Twenty-first International Conference on Machine Learning*, page 104.
- Van Der Vaart, A. and Wellner, J. (2000). *Weak Convergence and Empirical Processes: with Applications to Statistics (Springer Series in Statistics)*. Springer, corrected edition.
- Wang, J.-L., Xue, L., Zhu, L., and Chong, Y. S. (2010). Estimation for a partial-linear single-index model. *The Annals of Statistics*, 38(1):246–274.
- Xia, Y. (2006). Asymptotic distributions for two estimators of the single-index model. *Econometric Theory*, 22(6):1112–1137.
- Xia, Y. (2007). A constructive approach to the estimation of dimension reduction directions. *The Annals of Statistics*, 35(6):2654–2690.
- Xia, Y. and Li, W. K. (1999). On single-index coefficient regression models. *Journal of the American Statistical Association*, 94(448):1275–1285.
- Xia, Y., Tong, H., Li, W. K., and Zhu, L.-X. (2009). An adaptive estimation of dimension reduction space. In *Exploration of a Nonlinear World: An Appreciation of Howell Tong’s Contributions to Statistics*, pages 299–346. World Scientific.
- Ying, C. and Yu, Z. (2020). Fréchet sufficient dimension reduction for random objects. *arXiv preprint arXiv:2007.00292*.
- Yu, Y. and Ruppert, D. (2002). Penalized spline estimation for partially linear single-index

- models. *Journal of the American Statistical Association*, 97(460):1042–1054.
- Zhang, H.-Y., Wang, S.-J., Liu, B., Ma, Z.-L., Yang, M., Zhang, Z.-J., and Teng, G.-J. (2010). Resting brain connectivity: changes during the progress of Alzheimer disease. *Radiology*, 256(2):598–606.
- Zhao, W., Zhang, F., Li, R., and Lian, H. (2020). Principal single-index varying-coefficient models for dimension reduction in quantile regression. *Journal of Statistical Computation and Simulation*, 90(5):800–818.
- Zhou, J. and He, X. (2008). Dimension reduction based on constrained canonical correlation and variable filtering. *The Annals of Statistics*, 36(4):1649–1668.
- Zhu, L. and Xue, L. (2006). Empirical likelihood confidence regions in a partially linear single-index model. *Journal of the Royal Statistical Society: Series B (Statistical Methodology)*, 68(3):549–570.
- Zhu, L.-P. and Zhu, L.-X. (2009). On distribution-weighted partial least squares with diverging number of highly correlated predictors. *Journal of the Royal Statistical Society: Series B (Statistical Methodology)*, 71(2):525–548.

Supplementary Material

S.1. Proofs and additional results

Proof of Proposition 2. By Assumption (A2), $m_{\oplus}(\mathbf{x}^{\top} \bar{\boldsymbol{\theta}})$ is a continuous function of $\bar{\boldsymbol{\theta}}$ for all $\bar{\boldsymbol{\theta}} \in \bar{\Theta}$ for almost all \mathbf{x} on the compact ball $\bar{\Theta}$. This implies $m_{\oplus}(\mathbf{x}^{\top} \bar{\boldsymbol{\theta}})$ is uniformly continuous in $\bar{\boldsymbol{\theta}} \in \bar{\Theta}$ for almost all \mathbf{x} . That is, there exists $\delta > 0$ for any $\varepsilon > 0$ and $\bar{\boldsymbol{\theta}}_1, \bar{\boldsymbol{\theta}}_2 \in \bar{\Theta}$ such that $\|\bar{\boldsymbol{\theta}}_1 - \bar{\boldsymbol{\theta}}_2\| \leq \delta$, implies $d(m_{\oplus}(\mathbf{x}^{\top} \bar{\boldsymbol{\theta}}_1), m_{\oplus}(\mathbf{x}^{\top} \bar{\boldsymbol{\theta}}_2)) \leq \varepsilon$ for almost all \mathbf{x} . This also results in the uniform continuity of $d^2(y, m_{\oplus}(\mathbf{x}^{\top} \bar{\boldsymbol{\theta}}))$ as a function of $\bar{\boldsymbol{\theta}}$, for all $\bar{\boldsymbol{\theta}} \in \bar{\Theta}$ for almost all \mathbf{x}, y . To observe this, let $\bar{\boldsymbol{\theta}}_1, \bar{\boldsymbol{\theta}}_2 \in \bar{\Theta}$ such that $\|\bar{\boldsymbol{\theta}}_1 - \bar{\boldsymbol{\theta}}_2\| \rightarrow 0$.

$$\begin{aligned} & |d^2(y, m_{\oplus}(\mathbf{x}^{\top} \bar{\boldsymbol{\theta}}_1)) - d^2(y, m_{\oplus}(\mathbf{x}^{\top} \bar{\boldsymbol{\theta}}_2))| \\ &= |d(y, m_{\oplus}(\mathbf{x}^{\top} \bar{\boldsymbol{\theta}}_1)) + d(y, m_{\oplus}(\mathbf{x}^{\top} \bar{\boldsymbol{\theta}}_2))| |d(y, m_{\oplus}(\mathbf{x}^{\top} \bar{\boldsymbol{\theta}}_1)) - d(y, m_{\oplus}(\mathbf{x}^{\top} \bar{\boldsymbol{\theta}}_2))| \\ &\leq (|d(y, m_{\oplus}(\mathbf{x}^{\top} \bar{\boldsymbol{\theta}}_1))| + |d(y, m_{\oplus}(\mathbf{x}^{\top} \bar{\boldsymbol{\theta}}_2))|) |d(y, m_{\oplus}(\mathbf{x}^{\top} \bar{\boldsymbol{\theta}}_1)) - d(y, m_{\oplus}(\mathbf{x}^{\top} \bar{\boldsymbol{\theta}}_2))| \\ &\leq 2D |d(y, m_{\oplus}(\mathbf{x}^{\top} \bar{\boldsymbol{\theta}}_1)) - d(y, m_{\oplus}(\mathbf{x}^{\top} \bar{\boldsymbol{\theta}}_2))| \leq 2Dd(m_{\oplus}(\mathbf{x}^{\top} \bar{\boldsymbol{\theta}}_1), m_{\oplus}(\mathbf{x}^{\top} \bar{\boldsymbol{\theta}}_2)) \rightarrow 0. \end{aligned}$$

This holds for almost all \mathbf{x}, y . The second inequality uses the assumption that Ω has diameter D and the last inequality follows from the triangle inequality property of the metric d . The above technique is going to be used often in the subsequent proofs. Thus, by bounded convergence, $\mathbb{E}(d^2(Y, m_{\oplus}(\mathbf{X}^{\top} \bar{\boldsymbol{\theta}})))$ is a continuous function of $\bar{\boldsymbol{\theta}}$ for all $\bar{\boldsymbol{\theta}} \in \bar{\Theta}$. Hence the map $\bar{\boldsymbol{\theta}} \mapsto H(\bar{\boldsymbol{\theta}})$, $\bar{\boldsymbol{\theta}} \in \bar{\Theta}$ is continuous. Now, note that,

$$\begin{aligned} H(\bar{\boldsymbol{\theta}}) &= \mathbb{E}(d^2(Y, m_{\oplus}(\mathbf{X}^{\top} \bar{\boldsymbol{\theta}}))) = \mathbb{E}(\mathbb{E}(d^2(Y, m_{\oplus}(\mathbf{x}^{\top} \bar{\boldsymbol{\theta}})) | \mathbf{X} = \mathbf{x})) \\ &\geq \mathbb{E}(\mathbb{E}(d^2(Y, m_{\oplus}(\mathbf{x}^{\top} \bar{\boldsymbol{\theta}}_0)) | \mathbf{X} = \mathbf{x})) = \mathbb{E}(d^2(Y, m_{\oplus}(\mathbf{X}^{\top} \bar{\boldsymbol{\theta}}_0))) = H(\bar{\boldsymbol{\theta}}_0) \end{aligned}$$

The inequality follows since the existence of conditional Fréchet mean as a unique minimizer of the conditional Fréchet objective function is assumed. Thus $\bar{\boldsymbol{\theta}}_0 = \underset{\bar{\boldsymbol{\theta}} \in \bar{\Theta}}{\operatorname{argmin}} H(\bar{\boldsymbol{\theta}})$, for all $\bar{\boldsymbol{\theta}} \in \bar{\Theta}$. Similarly, by the definition of the local Fréchet regression estimator as a minimizer of the empirical weighted Fréchet mean (see (6)), one can show that $V_n(\hat{\boldsymbol{\theta}}) \leq V_n(\bar{\boldsymbol{\theta}})$ for all $\bar{\boldsymbol{\theta}} \in \bar{\Theta}$. \square

Throughout the proof, the notation \rightsquigarrow represents weak convergence as per (Van Der Vaart and Wellner, 2000), and $\ell^\infty(\Omega)$ denotes the space of bounded functions on Ω . The ordinary Euclidean norm on \mathbb{R}^p will be denoted by $\|\cdot\|$ and the Frobenius norm by $\|\cdot\|_F$.

Proof of Theorem 1. Recall that $\bar{\boldsymbol{\theta}} = (\theta_1, \boldsymbol{\theta})^{\top}$, for all $\bar{\boldsymbol{\theta}} \in \bar{\Theta}$. It is important to note that $\boldsymbol{\theta}_0$, $\tilde{\boldsymbol{\theta}}$, and $\hat{\boldsymbol{\theta}}$ are the unconstrained minimizers for the criteria functions $H(\cdot)$, $\tilde{V}_n(\cdot)$, and $V_n(\cdot)$ respectively. Thus we can view $H(\cdot)$, $\tilde{V}_n(\cdot)$, and $V_n(\cdot)$ to be effectively only functions of $\boldsymbol{\theta}$,

$\boldsymbol{\theta}^\top \boldsymbol{\theta} < 1$. Thus, if we can show $\hat{\boldsymbol{\theta}} - \boldsymbol{\theta}_0 \xrightarrow{P} 0$, using the facts that $\theta_{01} = \sqrt{1 - \|\boldsymbol{\theta}_0\|^2}$ and $\hat{\theta}_1 = \sqrt{1 - \|\hat{\boldsymbol{\theta}}\|^2}$, a simple application of continuous mapping theorem will yield the result that $\hat{\boldsymbol{\theta}} - \bar{\boldsymbol{\theta}}_0 \xrightarrow{P} 0$.

It is shown that the map $\boldsymbol{\theta} \mapsto H(\boldsymbol{\theta})$ is continuous and $\boldsymbol{\theta}_0$ and $\hat{\boldsymbol{\theta}}$ are the respective unique minimizers of $H(\boldsymbol{\theta})$ and $V_n(\boldsymbol{\theta})$. By Corollary 3.2.3 in [Van Der Vaart and Wellner \(2000\)](#) it is then sufficient to show the convergence of $\sup_{\boldsymbol{\theta}} \|V_n(\boldsymbol{\theta}) - H(\boldsymbol{\theta})\|$, to zero in probability. To do this we first show that $V_n \rightsquigarrow H$ in $\ell^\infty(\Omega)$ and apply Theorem 1.3.6 of [Van Der Vaart and Wellner \(2000\)](#). The weak convergence result is proved (see Theorem 1.5.4 of [Van Der Vaart and Wellner \(2000\)](#)) by checking that

$$(C1) \quad V_n(\boldsymbol{\theta}) - H(\boldsymbol{\theta}) = o_P(1) \text{ for all } \boldsymbol{\theta},$$

(C2) V_n is asymptotically equi-continuous in probability, that is, for all $\epsilon, \eta > 0$, there exists

$$\delta > 0 \text{ such that, } \limsup_{n \rightarrow \infty} P \left[\sup_{\|\boldsymbol{\theta}_1 - \boldsymbol{\theta}_2\| \leq \delta} |V_n(\boldsymbol{\theta}_1) - V_n(\boldsymbol{\theta}_2)| > \epsilon \right] < \eta.$$

We first express the difference between the sample and population objective functions as the sum of two differences by introducing the intermediate quantity $\tilde{V}_n(\cdot)$ as described in (4). Recalling $\tilde{V}_n(\boldsymbol{\theta}) := \frac{1}{M} \sum_{l=1}^M d^2(\tilde{Y}_l, m_{\oplus}(\tilde{\mathbf{X}}_l^\top \boldsymbol{\theta}))$,

$$\|V_n(\boldsymbol{\theta}) - H(\boldsymbol{\theta})\| = |V_n(\boldsymbol{\theta}) - \tilde{V}_n(\boldsymbol{\theta})| + |\tilde{V}_n(\boldsymbol{\theta}) - H(\boldsymbol{\theta})|. \quad (28)$$

Now,

$$|\tilde{V}_n(\boldsymbol{\theta}) - H(\boldsymbol{\theta})| = \left| \frac{1}{M} \sum_{l=1}^M d^2(\tilde{Y}_l, m_{\oplus}(\tilde{\mathbf{X}}_l^\top \boldsymbol{\theta})) - \mathbb{E}(d^2(Y, m_{\oplus}(\mathbf{X}^\top \boldsymbol{\theta}))) \right| = o_P(1),$$

by Weak Law of Large Numbers, since $\tilde{V}_n(\cdot)$ can be seen as an i.i.d sum. As for the first term in (28),

$$\begin{aligned} |V_n(\boldsymbol{\theta}) - \tilde{V}_n(\boldsymbol{\theta})| &= \left| \frac{1}{M} \sum_{l=1}^M d^2(\tilde{Y}_l, \hat{m}_{\oplus}(\tilde{\mathbf{X}}_l^\top \boldsymbol{\theta})) - \frac{1}{M} \sum_{l=1}^M d^2(\tilde{Y}_l, m_{\oplus}(\tilde{\mathbf{X}}_l^\top \boldsymbol{\theta})) \right| \\ &\leq 2D \frac{1}{M} \sum_{l=1}^M d(\hat{m}_{\oplus}(\tilde{\mathbf{X}}_l^\top \boldsymbol{\theta}), m_{\oplus}(\tilde{\mathbf{X}}_l^\top \boldsymbol{\theta})). \end{aligned} \quad (29)$$

The steps to obtain (29) are similar to those followed in the proof of Proposition 2, using the total boundedness of Ω and properties of the metric d .

It remains to show $\frac{1}{M} \sum_{l=1}^M d(\hat{m}_\oplus(\tilde{\mathbf{X}}_l^\top \boldsymbol{\theta}), m_\oplus(\tilde{\mathbf{X}}_l^\top \boldsymbol{\theta})) \xrightarrow{P} 0$. Observe that,

$$\frac{1}{M} \sum_{l=1}^M d(\hat{m}_\oplus(\tilde{\mathbf{X}}_l^\top \boldsymbol{\theta}), m_\oplus(\tilde{\mathbf{X}}_l^\top \boldsymbol{\theta})) \leq \frac{1}{M} \sum_{l=1}^M \sup_t d(\hat{m}_\oplus(t), m_\oplus(t)) = \frac{1}{M} \sum_{l=1}^M O_P(a_n) = o_P(1), \quad (30)$$

where a_n is the rate of uniform convergence for the local Fréchet regression estimate, as given in (11) for Lemma 1 (Chen and Müller, 2020). We use here that the O_P terms in the sum are uniform in l . Hence the result follows. Thus we have (C1). The finite distribution converges weakly since, for any $k \in \mathcal{N}$ and $\boldsymbol{\theta}_1, \dots, \boldsymbol{\theta}_k \in \Theta$, we have $(V_n(\boldsymbol{\theta}_1), \dots, V_n(\boldsymbol{\theta}_k)) \rightsquigarrow (H(\boldsymbol{\theta}_1), \dots, H(\boldsymbol{\theta}_k))$.

Here, it is also important to observe that, by virtue of Lemma 1,

$$\begin{aligned} & \sup_{\boldsymbol{\theta} \in \Theta} |V_n(\boldsymbol{\theta}) - \tilde{V}_n(\boldsymbol{\theta})| \\ & \leq \sup_{\boldsymbol{\theta} \in \Theta} \frac{1}{M} \sum_{l=1}^M d(\hat{m}_\oplus(\tilde{\mathbf{X}}_l^\top \boldsymbol{\theta}), m_\oplus(\tilde{\mathbf{X}}_l^\top \boldsymbol{\theta})) \leq \frac{1}{M} \sum_{l=1}^M \sup_{\tilde{\mathbf{X}}_l^\top \boldsymbol{\theta} \in \mathbb{R}} d(\hat{m}_\oplus(\tilde{\mathbf{X}}_l^\top \boldsymbol{\theta}), m_\oplus(\tilde{\mathbf{X}}_l^\top \boldsymbol{\theta})) = O_P(a_n). \end{aligned} \quad (31)$$

For (C2), let $\epsilon, \gamma > 0$ and $\boldsymbol{\theta}_1, \boldsymbol{\theta}_2 \in \Theta$.

$$\begin{aligned} & P \left[\sup_{\|\boldsymbol{\theta}_1 - \boldsymbol{\theta}_2\| \leq \delta} |V_n(\boldsymbol{\theta}_1) - V_n(\boldsymbol{\theta}_2)| > \epsilon \right] \\ & \leq P \left[\sup_{\|\boldsymbol{\theta}_1 - \boldsymbol{\theta}_2\| \leq \delta} |V_n(\boldsymbol{\theta}_1) - \tilde{V}_n(\boldsymbol{\theta}_1)| > \frac{\epsilon}{3} \right] + P \left[\sup_{\|\boldsymbol{\theta}_1 - \boldsymbol{\theta}_2\| \leq \delta} |V_n(\boldsymbol{\theta}_2) - \tilde{V}_n(\boldsymbol{\theta}_2)| > \frac{\epsilon}{3} \right] \\ & \quad + P \left[\sup_{\|\boldsymbol{\theta}_1 - \boldsymbol{\theta}_2\| \leq \delta} |\tilde{V}_n(\boldsymbol{\theta}_1) - \tilde{V}_n(\boldsymbol{\theta}_2)| > \frac{\epsilon}{3} \right] \end{aligned} \quad (32)$$

Using (31), the first two terms of (32) are $O_P(a_n) = o_P(1)$, uniformly in $\boldsymbol{\theta}_1$ and $\boldsymbol{\theta}_2$ respectively. For the third term,

$$P \left[\sup_{\|\boldsymbol{\theta}_1 - \boldsymbol{\theta}_2\| \leq \delta} |\tilde{V}_n(\boldsymbol{\theta}_1) - \tilde{V}_n(\boldsymbol{\theta}_2)| > \frac{\epsilon}{3} \right] \leq P \left[\sup_{\|\boldsymbol{\theta}_1 - \boldsymbol{\theta}_2\| \leq \delta} 2D \frac{1}{M} \sum_{l=1}^M d(m_\oplus(\tilde{\mathbf{X}}_l^\top \boldsymbol{\theta}_1), m_\oplus(\tilde{\mathbf{X}}_l^\top \boldsymbol{\theta}_2)) > \frac{\epsilon}{3} \right] \quad (33)$$

By the assumption on $m_\oplus(\cdot)$ being K -Lipschitz continuous (see assumption (A2)) \mathbf{X} having a bounded support, (see assumption (R1)-(R2)), choosing $\delta < \frac{\epsilon}{6DK_1} : K_1 := K \|\tilde{\mathbf{X}}_l\|$, we have, (33) $\rightarrow 0$, as $\delta \rightarrow 0$. The asymptotic equi-continuity result for the stochastic process

$V_n(\boldsymbol{\theta})$, $\boldsymbol{\theta} \in \mathbb{R}^{p-1}$ and $\boldsymbol{\theta}^\top \boldsymbol{\theta} \leq 1$, follows. \square

Proof of Corollary 1. For any $\mathbf{x} \in \mathbb{R}^p$, we observe that, by the triangle inequality of the metric,

$$d(\hat{m}_\oplus(\mathbf{x}^\top \hat{\boldsymbol{\theta}}), m_\oplus(\bar{\boldsymbol{\theta}}_0)) \leq d(\hat{m}_\oplus(\mathbf{x}^\top \hat{\boldsymbol{\theta}}), m_\oplus(\hat{\boldsymbol{\theta}})) + d(m_\oplus(\mathbf{x}^\top \hat{\boldsymbol{\theta}}), m_\oplus(\bar{\boldsymbol{\theta}}_0)) \quad (34)$$

From Lemma 1, we know that

$$\sup_t d(\hat{m}_\oplus(t), m_\oplus(t)) = O_P(a_n) = o_P(1),$$

where a_n is as defined in (11). Since $\hat{\boldsymbol{\theta}}$ lies in a small neighborhood around $\bar{\boldsymbol{\theta}}_0$ for n large enough, the first term of (34) converges to zero in probability. Note that by Assumption (A2), $m_\oplus(\cdot)$ is continuous. Since, by Theorem 1 $\hat{\boldsymbol{\theta}} \xrightarrow{P} \bar{\boldsymbol{\theta}}_0$, using continuous mapping theorem, the second term of (34) also converges to zero in probability. The result follows using Slutsky's theorem. \square